Test Beam Studies of the Gas Mixtures
Ar:N$_2$:CH$_4$=91:4:5
Ar:CO$_2$:CH$_4$=92:5:3
Ar:CO$_2$:CH$_4$=93:4:3
Ar:CO$_2$:N$_2$:CF$_4$=95:2:2:1
for Drift Tubes

M. Deile[1], J. Dubbert[1], M. Faessler[1], C. Gruhn[2], N. P. Hessey[1], A. Staude[1]

Abstract

We present results of the 1995 Muon Test Beam, obtained with drift tubes with anode wire diameters of 30, 50, 70 and 160 μm. Measurements with high energy muons are complemented with photon data, using ^{55}Fe and ^{241}Am sources. The data was taken at the nominal MDT pressure of 3 bar absolute, at zero magnetic field.

For each gas we give gas gain as a function of high voltage, and the fraction of limited streamers, as a function both of high voltage and of gas gain.

Streamer fractions are well below 1% at a gain of 2×10^4, for all gases and wire diameters. Only a weak dependence of the streamer fraction on the wire diameter was observed. Therefore the streamer fraction should have little influence on the choice of the wire diameter.

[1] Ludwig Maximilians University Munich
[2] Max Planck Institute Munich

Contents

1   Introduction

During the beam period in 1995 several gases for drift tubes were studied in the Muon test beam at CERN. Gas mixtures from previous years are now considered flammable which would demand high safety measures if they were to be used in ATLAS. All four gas mixtures we tested have the advantage that they are considered non-flammable by CERN standards at the present time.

The purpose of our measurements was to determine the suitability of the "new" gas mixtures for ATLAS MDT, as well as studying the influence of the wire diameter on streamer rates. In addition to the determination of gas gain and limited streamer rates we also studied maximum drift times and after-pulsing rates.

We studied the gases $Ar:N_2:CH_4=91:4:5$, $Ar:CO_2:CH_4=92:5:3$, $Ar:CO_2:CH_4=93:4:3$ and $Ar:CO_2:N_2:CF_4=95:2:2:1$ with single drift tubes equipped with anode wire of 30, 50, 70 and 160 μm diameter.

Measurements were made with high energy muons in the M2 beam line halo and with gamma sources (^{55}Fe and ^{241}Am) to study the differences in the results with different ionisation mechanism.

All measurements were made at zero magnetic field. We used the nominal MDT pressure of 3 bar absolute [1] for our studies.

The gases studied belong to three classes, all based on argon with small amounts of quencher.

The first gas contains nitrogen, which saturates the electron drift velocity, leading to a linear rt-relationship (space drift time relationship) and a maximum drift time around 480 ns. It has the disadvantage that the few streamers that do occur have a higher charge than streamers in gases without nitrogen. In addition the reaction $^{14}N(n,p)^{14}C$ can produce 600 keV protons (from background neutrons) inside the tube which contribute to the ageing. A pessimistic calculation (appendix A) indicates that the total deposited charge in the tubes might be increased by 20%.

The second gas contains CO_2, which reduces the streamer charge and the Lorentz angle. The rt-relationship is non-linear and the gas is slow (600 ns maximum drift time predicted by Garfield). The drift properties of gases containing CO_2 seem to be strongly influenced by contaminations, especially water; drift times up to 850 ns were observed in several MDT detectors in the test beam.

The third gas is a derivative of the second, containing less CO_2, which leads to a slightly more linear rt-relationship. The influence of contaminations is reduced but was still significant.

The fourth gas is the only four component mixture we studied. It consists entirely of non-flammable components and provides a linear rt-relationship in a magnetic field of 0.6 T. At higher gains after-pulsing was observed. The influence of CF_4 on ageing has to be investigated.

A full description of the methods and the results can be found in [2] (in German).

The dependence of resolution and efficiency on wire diameter will be discussed in a separate note.
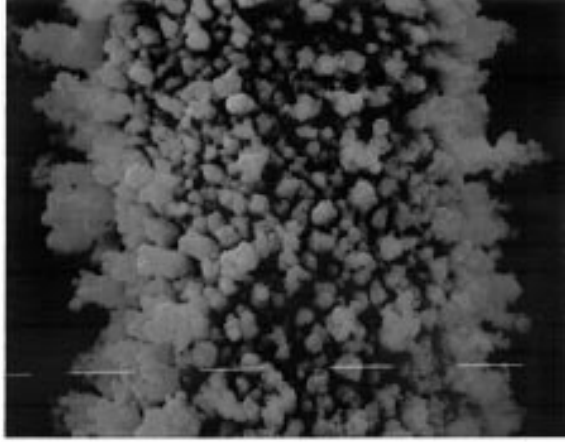
2   Setup

Figure 1: Experimental Setup

Fig. 1 shows the setup in the M2-Halo at CERN. The M2 area was built to test small to medium sized MDT prototypes with high energy muons, and offers the possibility to make studies inside magnetic fields. Trigger systems and several precision reference systems are available.

A coincidence of the four hodoscope planes constituted the main trigger for our beam measurements. The hodoscope planes covered an area of 1.4×1.4 m^2, each plane consisting of 16 partly overlapping scintillators. In addition a small scintillator (C1, 4×100 cm^2), mounted directly in front of the tubes, was put into coincidence with the hodoscope. For source measurements the signal itself was used to provide a trigger.

The drift tubes were placed inside a reference system of two Cathode Strip Chambers [3] and two Resistive Plate Chambers [4] for tracking.

The setup contained originally 6 tubes with 30, 40, 50, 70, 100 and 160 μm wires. The 40 μm tube was accidentally aged by a continuous discharge over a time period of 3 days prior to our measurements. The discharge was set up to burn away some contaminations in the tube which produced a Malter effect [5, p. 338]. In all our measurements this tube behaved as if it had a 65 μm wire. After the beam period we opened the tube and analysed the wire. The surface was covered uniformly with green crystalline structures. Fig. 2 shows a photograph of the wire surface. An analysis of the X-ray spectrum of the wire revealed a high concentration of chlorine and oxygen, apart from the expected Cu peak (the wire material was CuBe). We believe that the structures are crystals of CuCl$_2$ and Cu(OH)$_2$, possibly with water trapped inside the domes. The origin of the chlorine has to be investigated. The wire will be excluded from further discussions.

The 100 μm wire had no electrical contact to the pins in the end caps. Since no

Figure 2: Photograph of the 40 μm wire surface, see text for explanation. The reference bars are 10 μm long.

replacement was manufactured we substituted a second 50 μm tube. The 50 μm tubes will be designated 50 I and 50 II.

The five drift tubes studied had 30 mm outer diameter and 400 μm wall-thickness, and were made of an Al-Mn alloy with no cathode treatment. Table 1 gives an overview of the tube parameters.

Wire diam. [μm]	Tube length [cm]	Wire material	Wire tension [N]
30	100	WRe	1.2
50 I	110	CuBe	unknown
50 II	100	unknown	3.9
70	100	CuBe	2.9
160	100	CuBe	12.3

Table 1: Munich Single Tube Parameters

Each tube was equipped with separate front end electronics. At the HV end the termination resistor was chosen to match the tube impedance, thus minimising reflections at that tube end. The preamplifier side was terminated with a protection resistor and the input impedance of the preamplifier (22 Ω in our case), the sum being smaller than the tube impedance, leading to negative reflections at this end (transmission coefficient tube-termination greater than 1) [6]. This allows us to collect a bigger fraction of charge compared to equal terminations. Table 2 lists the passive electronic components, and fig. 3 shows the circuit diagram.

All tubes were equipped with the L3 preamplifier [7]. The L3 is a fast preamplifier originally built for the L3 wire chambers. It has the drawback that the output must be AC coupled. This coupling produces a shallow (5% of the peak amplitude) but very long (several micro seconds) undershoot. To avoid that the undershoot cancelled out the signal, we had to use short ADC gates that reject the undershoot. The short integration time leads to large correction factors to extrapolate the collected charge to the the total charge deposited on the wire. With our gate width we collected about 10–20% of the
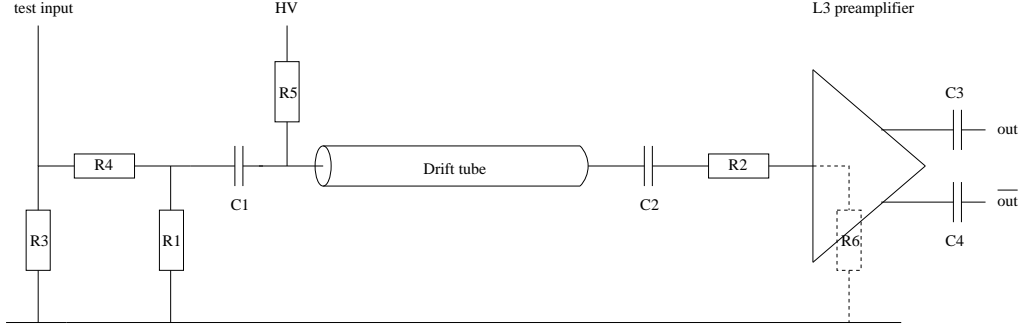
3

Figure 3: Circuit diagram of the tube electronics. R3 = 50 Ω, R4 = 100 kΩ, R5 = 1 MΩ, R6 = 22 Ω, C1 = C2 = 470 pF, C3 = C4 = 100 nF. The values of R1 and R2 are given in table 2.

Wire diam. [μm]	Termination HV side [Ω]	Termination pre amp side [Ω]
30	413	33 + R6
50 I	382	33 + R6
50 II	382	22 + R6
70	362	33 + R6
160	312	33 + R6

Table 2: Munich Single Tube passive electronic components

total charge. A careful calculation of the correction factors is necessary since the time derivatives are large. The L3 preamplifier has a gain of 24 mV/μA with a shaping time of 4 ns and provides a differential output. This shaping time is too short and the amplifier gain is too low to trigger comfortably on the 25th electron at a gas gain of 2×10^4, which is the current aim for ATLAS.

The read-out electronics aimed to provide both charge and time information. The non-inverted L3 output was duplicated in an active splitter box (essentially an emitter follower) and provided the analog ADC signal. After this duplication the differential signal was discriminated and provided the time information. We used a 48-channel L3 discriminator card [8]. Thresholds down to 5 mV, well below the recommended 20 mV were used. No oscillations or instabilities were observed. The analog signals were recorded with a charge sensitive LeCroy 2249W ADC. The time information was recorded using a LeCroy 2277 TDC, which allows up to 16 hits per channel. The multi-hit capability was used for simple after-pulsing studies. All discriminator and ADC channels were calibrated individually. Fig. 4 shows a schematic of the read-out electronics. The data acquisition system of the Muon test beam is described in [9].

The gas system used premixed bottles. The tubes were connected in parallel to the gas system, and the flow rate was adjusted to give 1 volume exchange every 6 hours. The pressure was measured with a high precision absolute pressure gauge and regulated via an electronic flow-control valve connected by a feedback loop (MKS Baratron 690, MKS 248 Valve and MKS 250 Controller Unit with MKS 270C Signal Conditioner). For all measurements the gas pressure was kept constant at 3 bar absolute with a rms deviation of 0.1%.
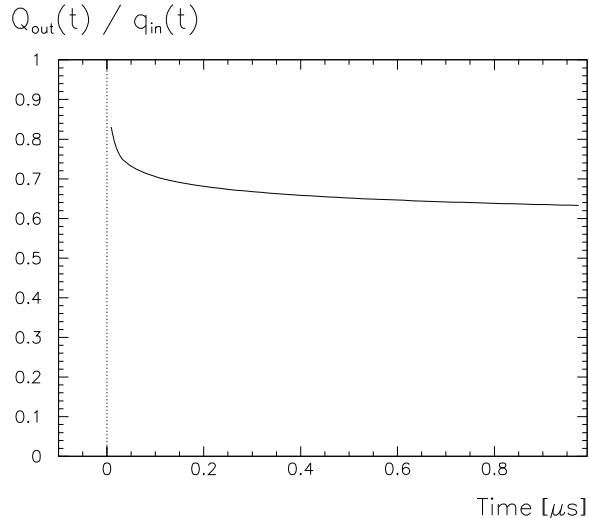
4

Figure 4: Schematic view of the read-out electronics for the Munich Single Tubes.

3 Gas gain measurements

3.1 Calculation of the Gas gain using ADC spectra

The gas gain G is defined as the ratio of the deposited charge on the wire and the primary charge. For a given track, the charge q_i of the i-th cluster generates a charge $G\,q_i$ when reaching the wire. If we ignore saturation effects, which are small for proportional mode signals at low rates, the gas gain is independent of the charge arriving at the wire. Therefore the total charge arriving at the wire from the track is

$$Q \;=\; G \sum_{cluster} q_i \;.$$
(1)

Some of the charge Q is lost at the HV end of the tube, and some of it arrives outside the ADC gate, so we collect only a smaller charge $Q_{col}(\tau)$ — which depends on the gate width τ — in the ADC.

Assuming a linear response of the electronics, $Q_{col}(\tau)$ is the sum of charges collected from the clusters,

$$Q_{col}(\tau) \;=\; G \sum_{cluster} q_{col}(\tau_i) \;=\; G \sum_{cluster} f(\tau_i)\, q_i \;,$$
(2)

where $\tau_i \equiv \tau - t_i$ with t_i the drift time of the i-th cluster to the wire, $q_{col}(\tau_i)$ is the charge seen by the ADC from the i-th cluster and

$$f(\tau_i) \;\equiv\; \frac{q_{col}(\tau_i)}{q_i}$$
(3)

is the fraction of the cluster charge that is collected. We write

$$f(\tau_i) \;=\; \frac{q_{col}(\tau_i)}{q_{ind,i}(\tau_i)}\, \frac{q_{ind,i}(\tau_i)}{q_i} \;,$$
(4)

5

$Q_{out}(t) / q_{in}(t)$

Time [μs]

Figure 5: Ratio of the charge collected by the pre amplifier and the induced charge on the wire.

where $q_{ind,i}(\tau_i)$ is the integral of the induced current on the wire in the effective gate width τ_i.

For the time range $0 \leq \tau_i \leq 1$ μs the ratio $q_{col}(\tau_i)/q_{ind,i}(\tau_i)$ is approximately independent of the collection time and the exact pulse shape. Fig. 5 shows this ratio (taken from [10], where pulse shapes and the charge fraction reaching the preamplifier are calculated). It will therefore be approximated by a constant, f, given in table 3.

Wire diam. [μm]	Correction factor f
30	0.64
50 I	0.63
50 II	0.64
70	0.62
160	0.58

Table 3: Approximate correction factors for pulse shaping and charge division.

The induced current on the wire, neglecting the electron component, is created by the drifting ion. Assuming a constant ion mobility the induced current for one single-charged ion is [5]:

$$I(t') = \begin{cases} \frac{e}{2\ln(b/a)} \frac{1}{t'+t_0} & (0 \leq t' \leq t_{max}) \\ 0 & \text{otherwise} \end{cases} \quad , \tag{5}$$

where e is the elementary charge, a the wire radius, b the inner tube radius and $t' \equiv t - t_i$ is the time since the cluster reached the wire. $t_{max} \equiv \ln(b/a)/2\mu V (b^2 - a^2)$ denotes the drift time of the ion to the tube wall. The time constant t_0 of the ion pulse is given by

$$t_0 = \frac{\ln(b/a)}{2\mu V} a^2 \ , \tag{6}$$

6

with μ being the ion mobility and V the applied high voltage.

Integrating (5) gives

$$q_{ind,i}(\tau_i) \;=\; \int_0^{\tau_i} n_i \, I(t') \, dt' \;=\; \frac{n_i \, e}{2\ln(b/a)} \ln\left(1 + \frac{\tau_i}{t_0}\right) \,, \tag{7}$$

where n_i is the number of electrons in the i-th cluster.

Regrouping (2), we get a measure of the gas gain for each track:

$$G \;=\; \frac{Q_{col}(\tau)}{f \sum q_{ind,i}(\tau_i)} \,. \tag{8}$$

With our assumption of no saturation effects the gain is independent of the primary charge, therefore (8) holds as well for the mean value taken over all possible tracks and therefore for the mean value over the tube:

$$G \;=\; \left\langle \frac{Q_{col}(\tau)}{f \sum q_{ind,i}(\tau_i)} \right\rangle \;=\; \frac{\langle Q_{col}(r) \rangle}{\langle f \sum q_{ind,i}(r_i) \rangle} \,, \tag{9}$$

where the angle brackets denote the average value over the tube. The last equality holds because we assumed a constant gain. For this case the collected charge is proportional to the primary charge for all radii; both are distributed with the same function, therefore the average of the ratio equals the ratio of the averages. We also introduced the explicit dependence of the collected charge on the track distance r from the wire; r_i denotes the distance of the i-th cluster from the wire.

Using the observable ADC value we can substitute the charge of the mean ADC value, $Q(\langle ADC \rangle)$ for the mean collected charge in (9):

$$G \;=\; \frac{Q(\langle ADC \rangle)}{\langle f \sum q_i(r_i) \rangle} \,. \tag{10}$$

The numerator was taken from the measured ADC spectra, see below.

The denominator was calculated by Monte Carlo methods. For the beam data, the calculation used Poisson distributed clusters along the track and the experimental clustersize distribution of argon, measured by Fischle et al. [11]. The mean value of 105 cluster/cm for the Poisson distribution was taken from [5] (for $\gamma = 1000$), scaled by a factor of 3 to account for our pressure of 3 bar absolute. We used a maximum cluster-size of 500 electrons. Although events with more than 30 electrons are very rare ($< 1\%$) they nevertheless contribute to the mean charge, as we have on average 250 clusters per track. The drift times of the individual clusters were calculated by linear interpolation of a Garfield simulation [12]. The Garfield results were scaled to match the observed maximum drift times (see section 5). For the source data the primary ionisation was calculated from the photon energy and the effective ionisation energy of argon (26 eV). The 5.9 keV ^{55}Fe photon produces 227 electron/ion pairs. The 59.8 keV photons of the ^{241}Am source are partly converted to 17.4 keV photons in an 0.4 mm thick Mo-foil. We used only the 17 keV peak with a primary ionisation of 670 electron/ion pairs, since the 60 keV photon liberates too much charge which leads to saturation effects. The clusters produced by ^{55}Fe photons were considered point-like, while those produced by ^{241}Am were smeared out radially by ± 0.5 mm from the creation point. Since the source data was taken with a self trigger, all electrons arrive at the same time relative to the gate and contributed

7
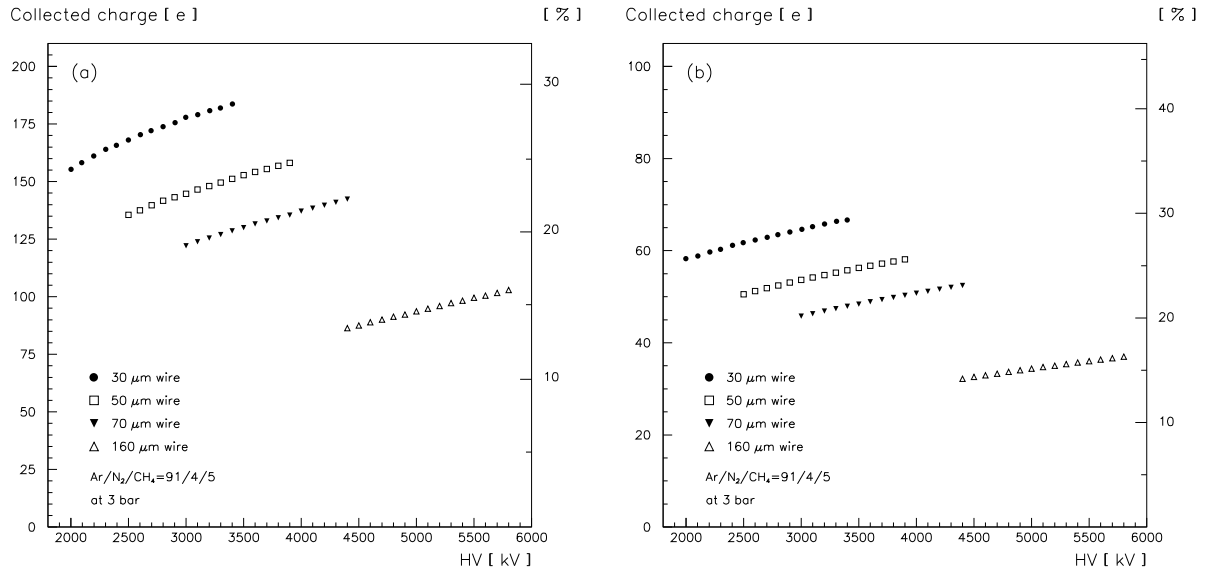
Figure 6: Collected charge dependence on HV for $Ar:N_2:CH_4=91:4:5$ at 3 bar. (a) for muons (550 ns gate width), (b) for ^{55}Fe-photons (250 ns gate width), ion mobility $= 0.512$ cm^2/Vs (Ar^+ in Ar at 3 bar), not corrected by $f(\tau_i)$.

the same fraction of collected charge, apart from the small effect of the smearing. Fig. 6 illustrates the dependence of the collected charge fraction on the HV for both beam and source data.

The dependence of the collected charge fraction for different wire diameters at a fixed HV follows from the dependence of t_0 (cf. eq. (6)) on the wire diameter. Neglecting the logarithmic term, t_0 depends quadratically on the wire diameter, with less charge collected for thicker wires.

As a final step we have to infer the mean collected charge from the mean ADC value in the measured ADC spectra. For beam data, we set the upper boundary for the mean by cutting off the streamer pulses and, following [5], the upper 5% in the ADC spectrum, fig. 7 (a). The lower boundary cuts off the pedestal. For source data, the peaks were fitted with a Gaussian and a second order background polynomial, fig. 7 (b).

Conversion of the ADC-value into the actual charge used a calibration curve for each channel. For the ADC calibration we fed pulses into the tubes via the test input (fig. 3) which is essentially a potential divider used to attenuate the output of a pulse generator. The ADC gate was triggered by the pulse itself. Only the differentiated edges of the test-pulse were transmitted by the AC coupled L3 preamplifier. The rise-time of the test pulses was chosen so that the undershoot of the pulse is rejected by the gate. We used 100 ns for the source measurements (300 ns gate length) and 300 ns for beam measurements (600-850 ns gate length). The charge Q_{calib} that arrives inside the ADC gate at the preamplifier input is approximately equal to the voltage drop across R_1 times the effective capacitance of the circuit (C_1 in series with C_2):

$$Q_{calib} \;=\; U_0 \, \frac{C_1 C_2}{C_1 + C_2} \, \frac{R_1}{R_1 + R_4} \;,\tag{11}$$
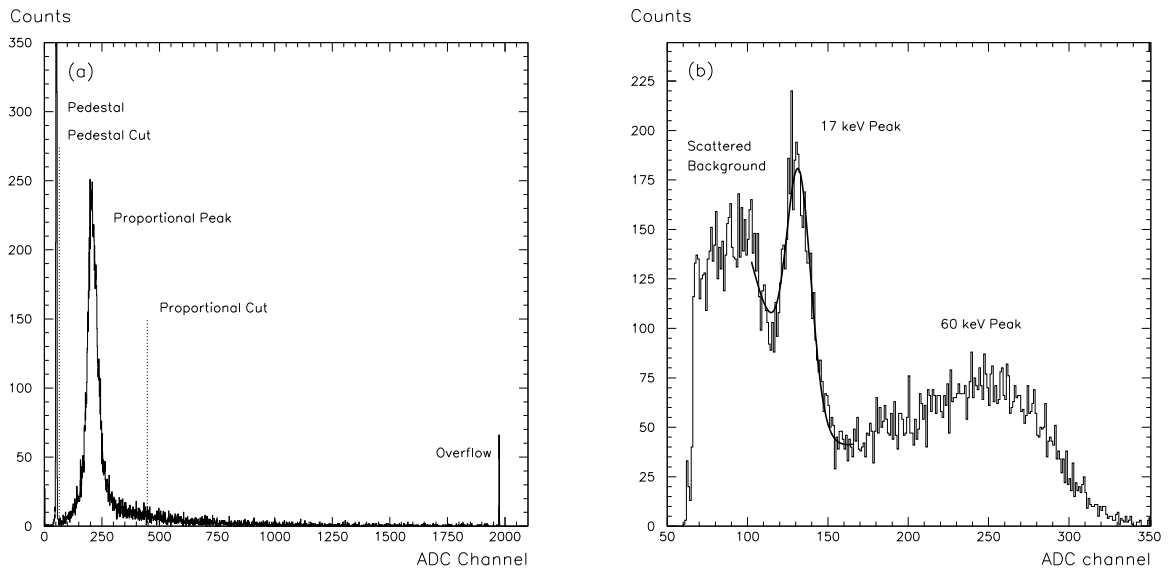
Figure 7: (a) Beam ADC spectrum and applied cuts, (b) ^{241}Am/Mo spectrum and fit (Gaussian + second order background polynomial).
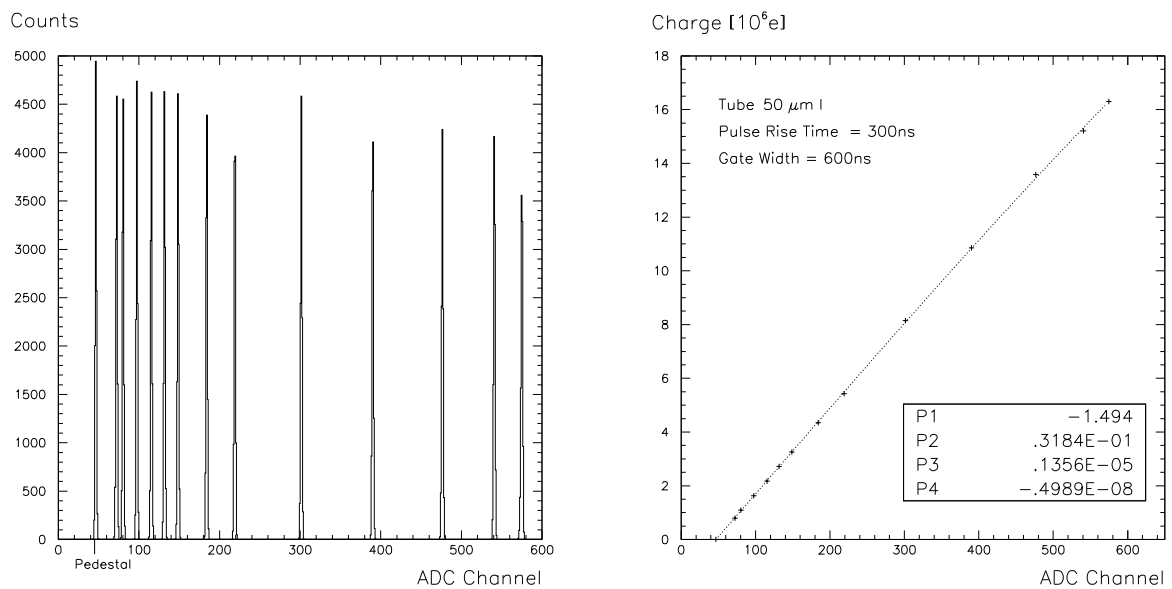
Figure 8: Example of an ADC calibration. Left: ADC spectrum of the test pulses, right: calibration curve (3rd order polynomial).

9

where U_0 denotes the input pulse amplitude, see fig. 3 for symbols. Corrections for the finite gate length, the wire resistance and the HV resistor are at the percent level. The pulse amplitude was varied to give different charges. The corresponding ADC values of 10000 pulses were recorded and calibration curves such as fig. 8 were produced.

The linear dependence of the charge on the ADC channel justifies the use of $Q(\langle ADC \rangle)$ instead of $\langle Q(ADC) \rangle$ in (10).

3.2 Gas gain measurement using current integration

An alternative way to measure the gas gain is to measure the current flowing in the tube with no preamplifier and decoupling capacitors. This method was tested by C. Sartena[1] with a one meter long drift tube of 3 cm outer radius, 400 μm wall thickness, equipped with a 50 μm wire [13]. The tube was mounted parallel to the M2 muon beam, 30 cm below the beam line. The parallel geometry maximises the primary ionisation of a muon in the tube by maximising the path length. The path length calculation took the beam profile, measured with two movable scintillators, into account. Background was suppressed by requiring the coincidence of two 10×10 cm^2 scintillators, mounted directly in front and behind the tube. The current drawn by the tube during a beam spill was measured as the voltage drop to ground across a 10 MΩ resistor. The current was converted into charge and the gain was calculated as the ratio of the measured charge, divided by the primary charge in the mean track length. A measurement was made for the Ar:N$_2$:CH$_4$=91:4:5 gas mixture and is in very good agreement with our results for low gas gains. The intrinsic problem with this kind of measurement is to know the muon flux through the tube precisely. For higher gas gains the current measurement overestimates the gain, because no distinction is made between limited streamer and proportional signals. If the streamer fraction and the ratio of streamer to proportional charge is known, this overestimate can be corrected.

4 Method of Streamer fraction measurement

4.1 Beam data

The number of streamer pulses for the beam measurements was estimated using an ADC-vs-TDC plot (fig. 9). We applied two cuts, one to cut off the pedestal, the second one to distinguish between proportional and streamer signals. Every hit between the two cuts was counted as a proportional signal, everything above the second cut as a streamer. To obtain an error estimate, we varied the cut position for the streamer by 50 ADC bins, but left the pedestal cut fixed, since it is well defined. The use of the 2d plot allowed us to take the Landau tail and delta-rays into account and approximately correct for them by shifting the cut to higher ADC values.

---

[1]Ludwig Maximilians University Munich
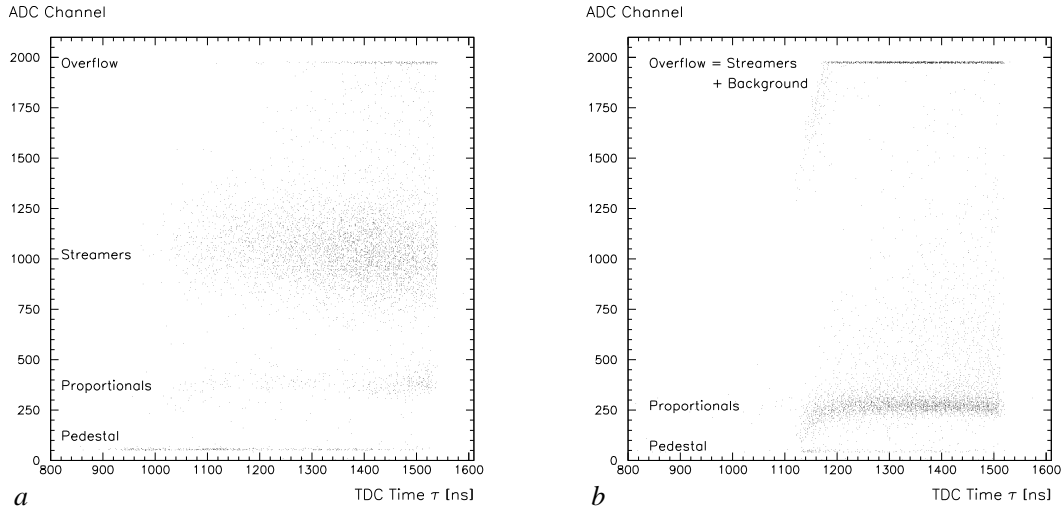
Figure 9: ADC versus TDC spectra. (a) Ar:CO_2:CH_4=93:4:3 at 3.7 kV, 3 bar, (b) Ar:CO_2:N_2:CF_4=95:2:2:1 at 3.7 kV, 3 bar, the linear rise to the overflow is due to the saturation of the L3 preamplifier. Smaller TDC times correspond to bigger distances.

4.2 Source data

For the source data there is, of course, no TDC spectrum, since we must use a self trigger of the signals. Therefore, we could only use the ADC spectra to decide where to cut. The method stays essentially the same as for the beam data. Two cuts, pedestal and streamer, are applied. The latter was varied by 50 ADC bins to obtain an error estimate. If the streamer charge is small, around 3-5 times the proportional mode charge, it becomes impossible to use the ^{241}Am source, since the streamer signals coincide with the 60 keV peak. This was the case for the Ar:CO_2:CH_4=93:4:3 gas. Only the ^{55}Fe source can then be used.

5 Maximum drift time measurements

The maximum drift times were obtained from the raw TDC spectra; t_0 corrections for the Hodoscope time reference were in the order of 1 ns and therefore negligible, as well as signal propagation times ($\leq$ 3 ns). Only the first hits were used, thus avoiding δ-electrons and after-pulses which might shift the drift times to bigger values. The values are extrapolations of the slope of the rising and falling edges to a bin-content of zero. Errors were estimated from the deviations of the bin contents from the mean slope and are around 10–15 ns. The measured results are compared with Garfield predictions.

11
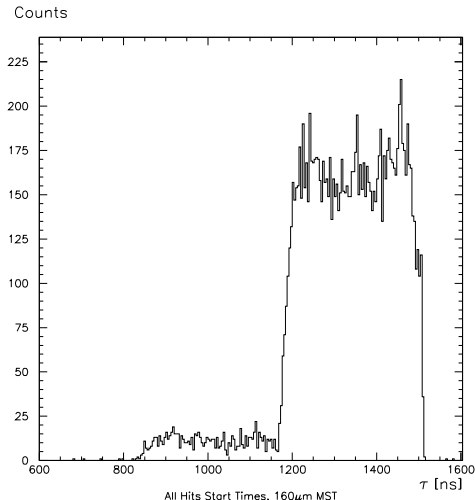
Figure 10: TDC spectrum of Ar:CO$_2$:N$_2$:CF$_4$=95:2:2:1 gas showing after-pulses, 160 μm wire at 5.3 kV, threshold 50 e^- (the direction of time is reversed).

6   After-pulsing studies

Photons created in the avalanche can travel to the cathode and eject electrons (photo effect), leading to a cluster of electrons near the tube wall. The cluster can drift to the wire and create a second avalanche, an after-pulse. The after-pulse spectrum thus starts after the maximum drift time, allowing a simple measure of the after-pulse rate. Fig. 10 shows a spectrum with after-pulses (TDC $<$ 1170 ns) as well as the hits due to primary ionisation (TDC $>$ 1170 ns). The ratio of hits in these regions gives a measure of the after-pulse rate. After-pulses are undesirable because they can create fake tracks in the detector. They also increase the total amount of deposited charge. The reduction of the life time however is small, since the cluster charge is typically much smaller than the primary ionisation. The method used here only counts clusters large enough to trigger the discriminator, which is the important statistic for tracking.

7   Results

In the following sections we present our results for each gas mixture. They start with the dependence of the gas gain on high voltage, followed by the limited streamer fraction dependence on gas gain and on high voltage. We indicate qualitatively the charge contained in a streamer pulse. Quantitative results are not possible due to the saturation of the L3 preamplifier and the limited range of the ADC. We then discuss the observed maximum drift times and compare them with Garfield [12] predictions. Finally the high voltages and gas gains for a level of 1% after-pulsing are given.

It is possible to extract the Diethorn parameters [5] of the gas from the "linear" part

12

of the log(Gain) vs HV curves. In the Diethorn model the parameter $\Delta\Phi$ plays the role of the potential difference necessary to create a new electron/ion pair (the ionisation energy divided by the elementary charge), and E_{min} is the minimum E-field to start the avalanche process. E_{min} scales with the pressure. With the assumption that the First Townsend coefficient depends linearly on the electric field, the gas gain G is given by:

$$\ln G \; = \; \frac{\ln 2}{\ln(b/a)} \frac{V}{\Delta\Phi} \; \ln \frac{V}{\ln(b/a)\, a\, E_{min}(\rho)} \; , \tag{12}$$

where V is the applied anode voltage, ρ is the gas density, a denotes the wire radius and b the inner tube radius.

The Diethorn parameters depend only on the properties of the gas mixture; they should be independent of the wire diameter.

At higher gain values a saturation of the gas gain was observed. The saturation was less for the ^{55}Fe than for the ^{241}Am and the beam. This effect was observed in all gas mixtures, suggesting that the total primary charge in the tube per track (227 e$^-$ for ^{55}Fe, 670 e$^-$ for ^{241}Am and around 600-700 e$^-$ for muons) is important for saturation effects, not the cluster sizes which are smaller for the muons than for the photons. This could result from the long ion drift times: the wire potential is shielded even for late coming electrons, resulting in a lower gain.

We observed systematic differences in the slopes of the gas gain curves for source and μ-beam data, the source curves being steeper. This effect might be caused by the undershoot of the preamplifier. In the long (beam) ADC gates the dependence of the ion-pulse time constant t_0 on the applied HV (shorter for higher voltages, see (6)) leads to different amounts of undershoot inside the gate. For lower voltages the gain is underestimated, for higher voltages it is overestimated, tilting the gain-HV curve. The short (source) ADC gates exclude almost all of the undershoot. As an example, fig. 11 shows the difference of the gas gains measured with ^{241}Am and muons for the Ar:N$_2$:CH$_4$=91:4:5 mixture. It should be noted that the data is consistent within the (systematic) errors. The different slopes of the Gain curves for beam and source data are also obvious in the Diethorn parameters. The beam data always exhibits a bigger $\Delta\Phi$ (inverse proportional
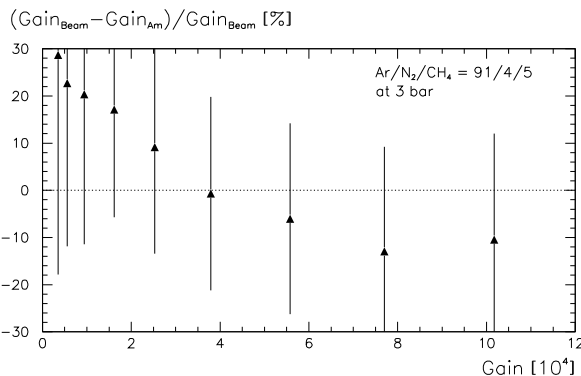
Figure 11: Difference of the gas gain measured with μ-beam and ^{241}Am/Mo, normalised to the μ-beam gas gain, for Ar:N$_2$:CH$_4$=91:4:5 at 3 bar.

to the slope of the curve) than the source data. The ^{241}Am and ^{55}Fe measurements are consistent with each other for all gases.

Error bars on the gain plots include random and systematic errors. Random errors are due to the uncertainties in the mean ADC-value. Systematic errors come from the ADC calibration and the calculated correction factors which include uncertainties from the primary ionisation, cluster size distribution, Garfield rt-relations, as well as contributions from pulse shaping and charge division factor. The overall systematic error is 10% of the gain value. At low gas gains the total error is dominated by the statistical contribution, at higher gains by the systematic part.

For the streamer fraction, the main uncertainty is in where to place the cut between streamer and proportional mode signals. The error bars were determined by studying the effect of moving this cut, see section 4.

7.1   Ar:N$_2$:CH$_4$=91:4:5

Fig. 12 shows the gas gain for the muon data. Two data sets were analysed to check the reproducibility of the method and are in excellent agreement with each other. Fig. 13 shows the HV-Gain plot for the ^{241}Am data, and fig. 14 compares the gas gain for beam, ^{241}Am and ^{55}Fe measurements for the 50 μm wires; also included is the data from the measurement of the tube current.

Tables 4, 5 and 6 list our results on the Diethorn parameters. The source measurements give different values from the beam measurements, but within a group the data is consistent.

Fig. 15 and fig. 16 show the measured streamer fractions, for the beam and ^{241}Am data. Fig. 17 compares all measurements for the 50 μm wires, including the ^{55}Fe data. The order of the streamer fraction for the source data is expected. The ^{241}Am photons produce bigger clusters (670 e^-) than the ^{55}Fe photons (227 e^-). Therefore the charge density is higher for the ^{241}Am cluster, favouring the creation of a limited streamer signal. The high streamer fraction in the μ-beam data is not well understood. For a gain of 2×10^4 the streamer fraction is well below 1% for all wire diameters. There is only a weak dependence of the streamer rate on the wire diameter. For easier comparison with measurements from other groups, fig. 18 and fig. 19 give the streamer fraction dependence on HV.

Unfortunately, we were not able to determine the charge contained in the limited streamer signal. The streamer signals end up in the ADC overflow. In addition, they saturated the L3 preamplifier. Therefore we are can only give a lower limit of 10 times the proportional charge for a limited streamer signal. Measurements by the Seattle group [14] indicate a factor of 70-130 for a similar mixture containing 5% N$_2$.

The Ar:N$_2$:CH$_4$=91:4:5 mixture has a very linear rt-relationship (fig. 20), with maximum drift times around 480 ns. The Garfield predictions are in good agreement with the observed values (the deviation around 5%), with Garfield being too slow for most HV and wire diameters. The maximum drift times are almost independent of the applied high voltage and the wire radius, see fig. 21. This behaviour is expected for a linear gas, since the electron drift velocity is saturated and does not depend on the electric field.

The Ar:N$_2$:CH$_4$=91:4:5 mixture shows no after-pulsing rates greater than 1% in the whole range of our measurements (up to a gas gain of 11×10^4).
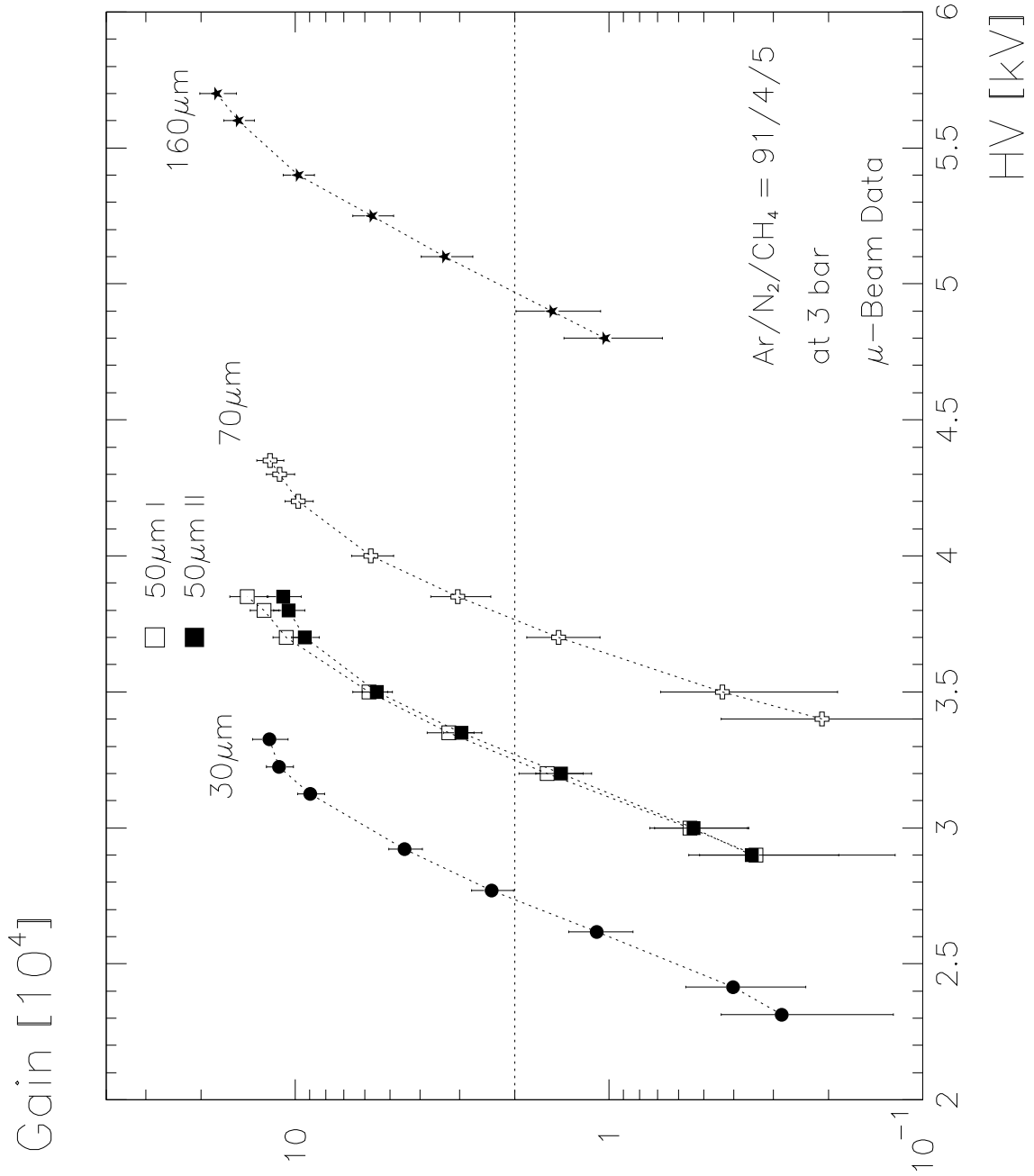
14

Figure 12: Gas gain versus HV for Ar:N$_2$:CH$_4$=91:4:5 at 3 bar, μ-beam data.
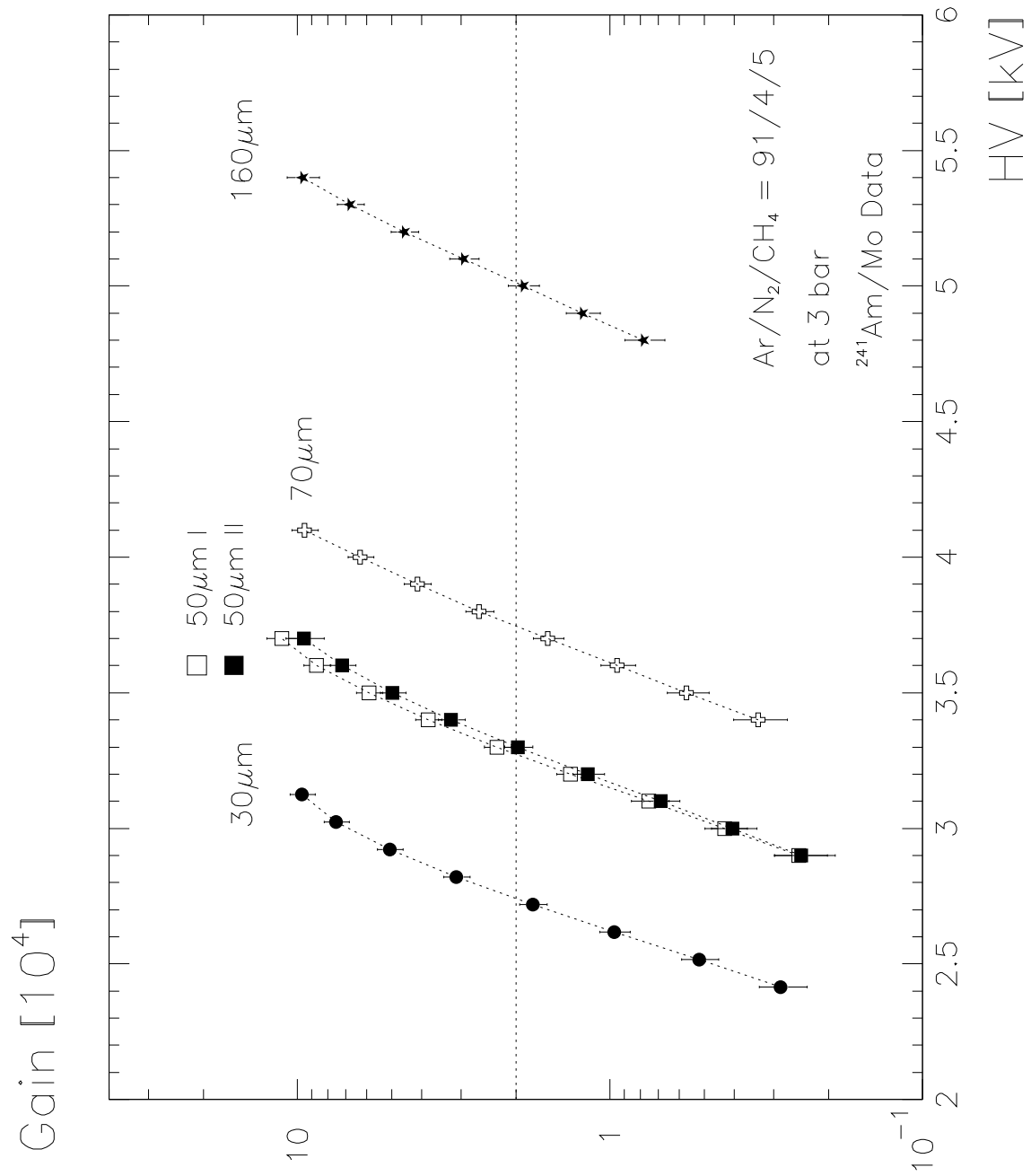
Figure 13: Gas gain versus HV for Ar:N$_2$:CH$_4$=91:4:5 at 3 bar, ^{241}Am/Mo data.
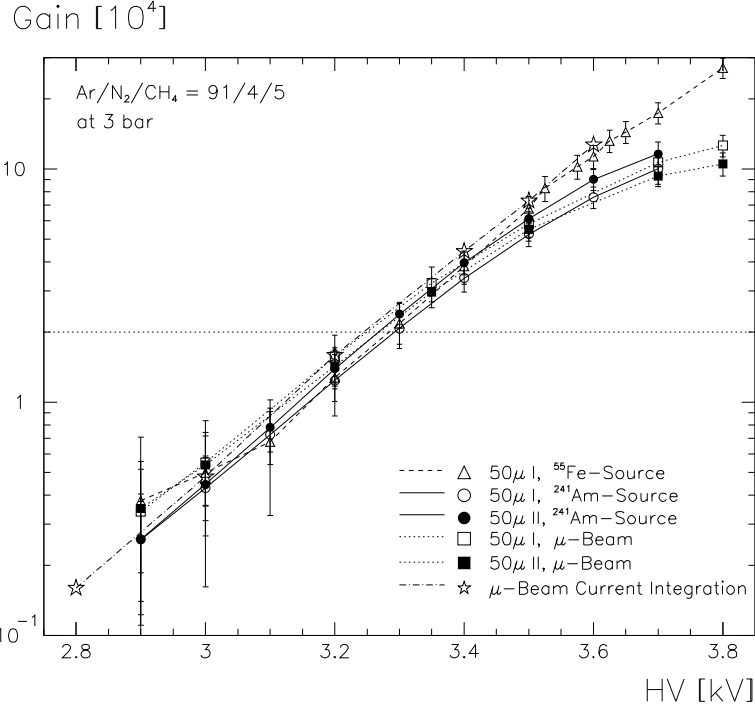
Figure 14: Comparison of the gas gain measurements for Ar:N$_2$:CH$_4$=91:4:5 at 3 bar, 50 μm wire.

Wire diam. [μm]	$\Delta\Phi$ [V]	E_{min}(3 bar) [kV/cm]	E_{min}(1 bar) [kV/cm]
30	51 $\pm$ 2	42 $\pm$ 3 $\pm$ 12	14 $\pm$ 1 $\pm$ 4
50 I	54 $\pm$ 1	46 $\pm$ 2 $\pm$ 8	15 $\pm$ 1 $\pm$ 3
50 II	59 $\pm$ 1	40 $\pm$ 1 $\pm$ 7	13 $\pm$ 0 $\pm$ 2
70	62 $\pm$ 7	43 $\pm$ 7 $\pm$ 9	14 $\pm$ 2 $\pm$ 3
160	69 $\pm$ 1	43 $\pm$ 1 $\pm$ 10	14 $\pm$ 0 $\pm$ 3

Table 4: Diethorn parameters for Ar:N$_2$:CH$_4$=91:4:5, μ-beam data.

Wire diam. [μm]	$\Delta\Phi$ [V]	E_{min}(3 bar) [kV/cm]	E_{min}(1 bar) [kV/cm]
30	38 $\pm$ 1	67 $\pm$ 2 $\pm$ 4	22 $\pm$ 1 $\pm$ 1
50 I	41 $\pm$ 1	66 $\pm$ 2 $\pm$ 4	22 $\pm$ 1 $\pm$ 1
50 II	46 $\pm$ 1	58 $\pm$ 2 $\pm$ 4	19 $\pm$ 1 $\pm$ 1
70	44 $\pm$ 1	65 $\pm$ 1 $\pm$ 4	22 $\pm$ 0 $\pm$ 1
160	54 $\pm$ 1	54 $\pm$ 1 $\pm$ 4	18 $\pm$ 0 $\pm$ 1

Table 5: Diethorn parameters for Ar:N$_2$:CH$_4$=91:4:5, ^{241}Am/Mo data.

Wire diam. [μm]	$\Delta\Phi$ [V]	E_{min}(3 bar) [kV/cm]	E_{min}(1 bar) [kV/cm]
50 I	44 $\pm$ 1	62 $\pm$ 2 $\pm$ 11	21 $\pm$ 1 $\pm$ 4

Table 6: Diethorn parameters for Ar:N$_2$:CH$_4$=91:4:5, ^{55}Fe data.
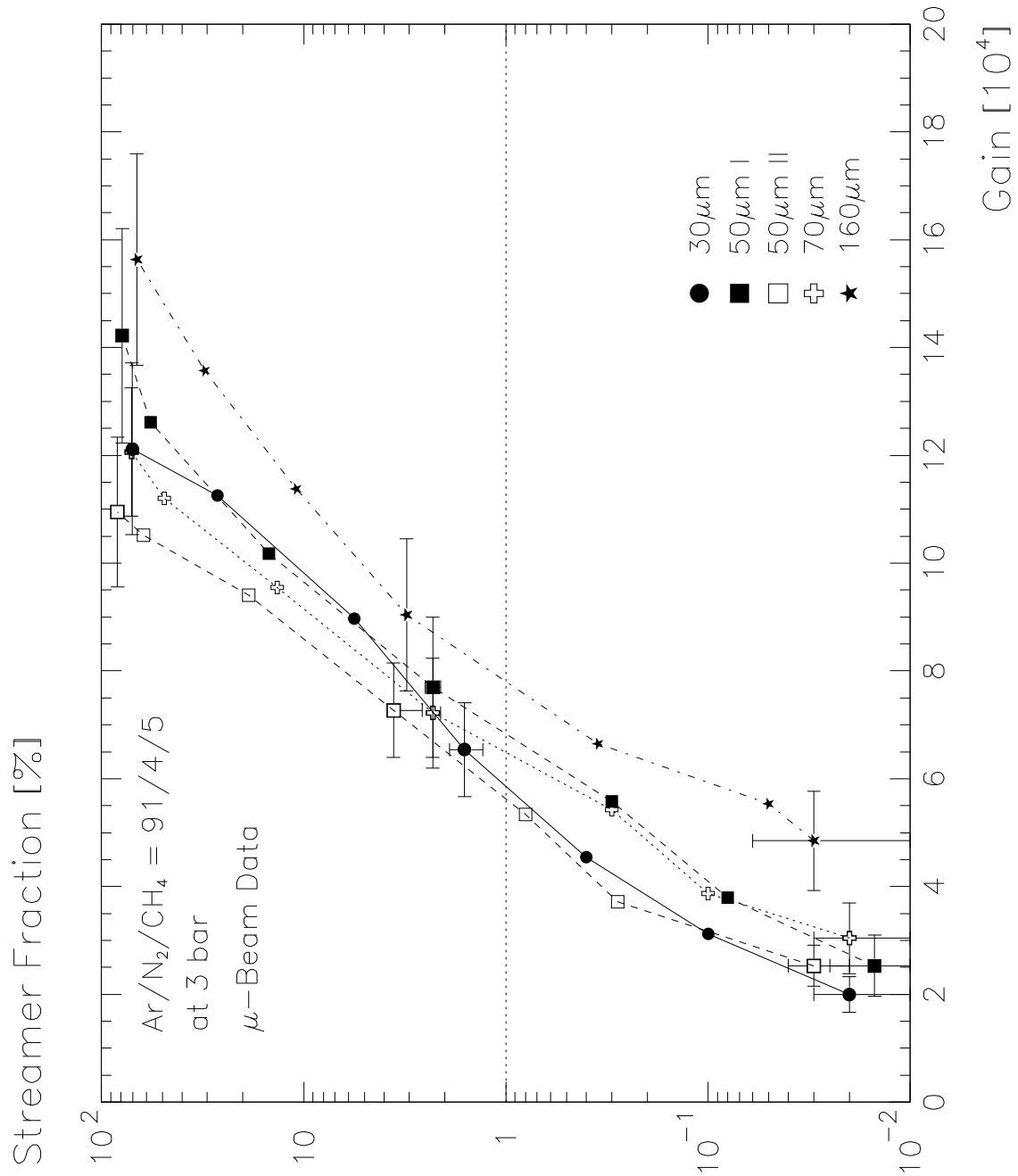
Figure 15: Limited streamer fraction versus gas gain, Ar:N$_2$:CH$_4$=91:4:5 at 3 bar, μ-beam data. Only a representative sample of error bars is shown.
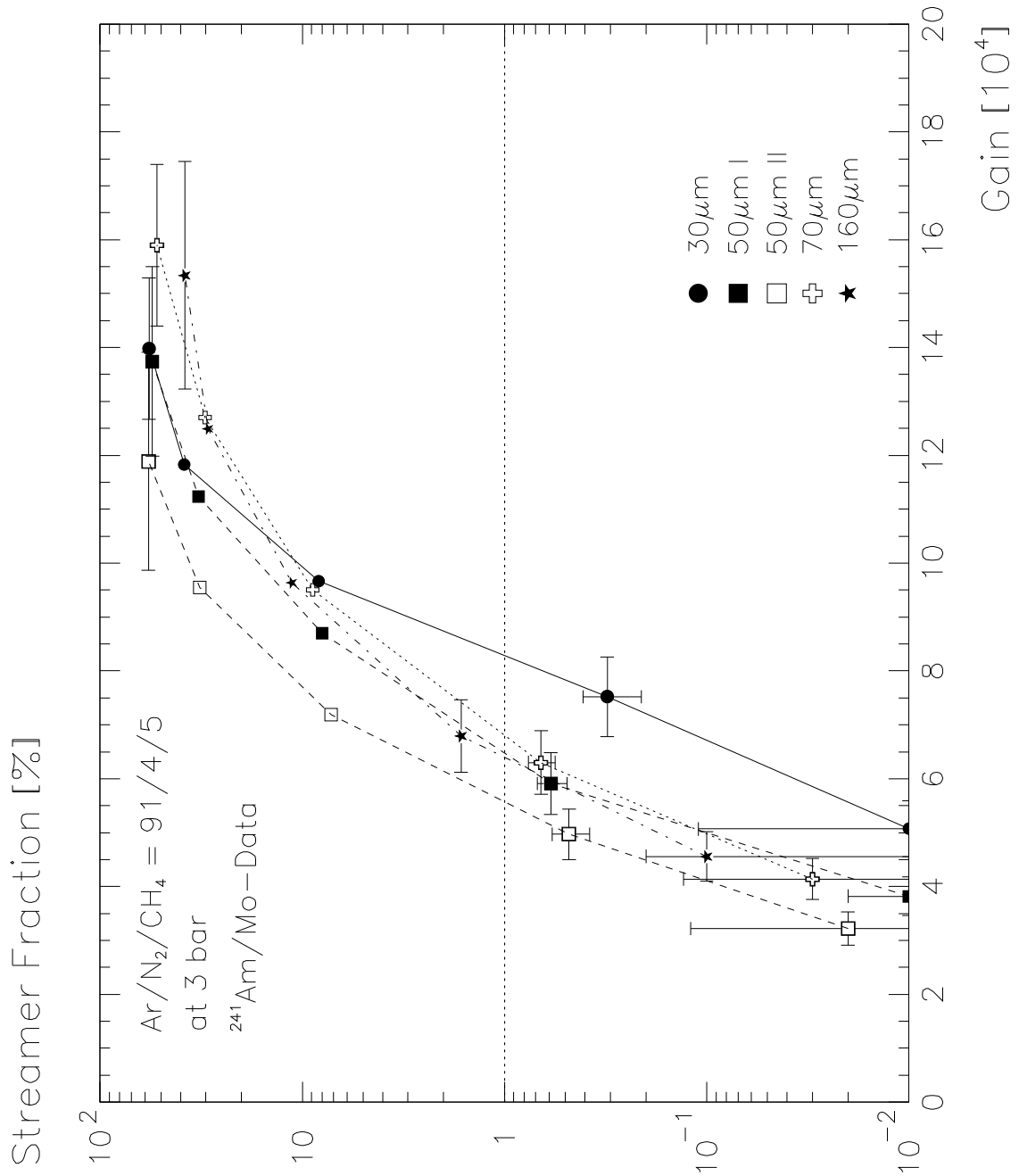
Figure 16: Limited streamer fraction versus gas gain, Ar:N$_2$:CH$_4$=91:4:5 at 3 bar, ^{241}Am/Mo data. Only a representative sample of error bars is shown.
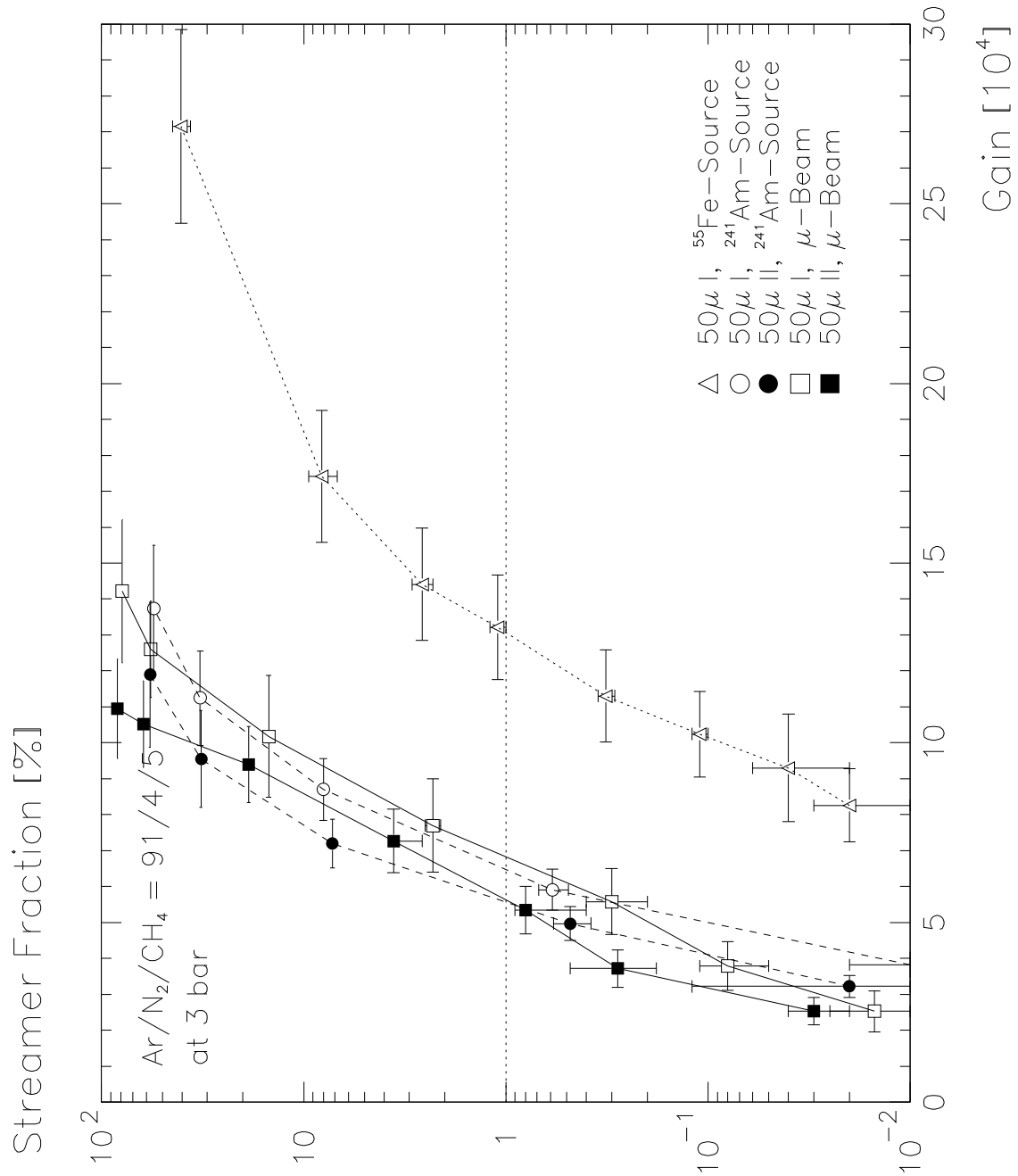
Figure 17: Comparison of the limited streamer fraction versus gas gain, Ar:N$_2$:CH$_4$=91:4:5 at 3 bar, 50 μm wire.
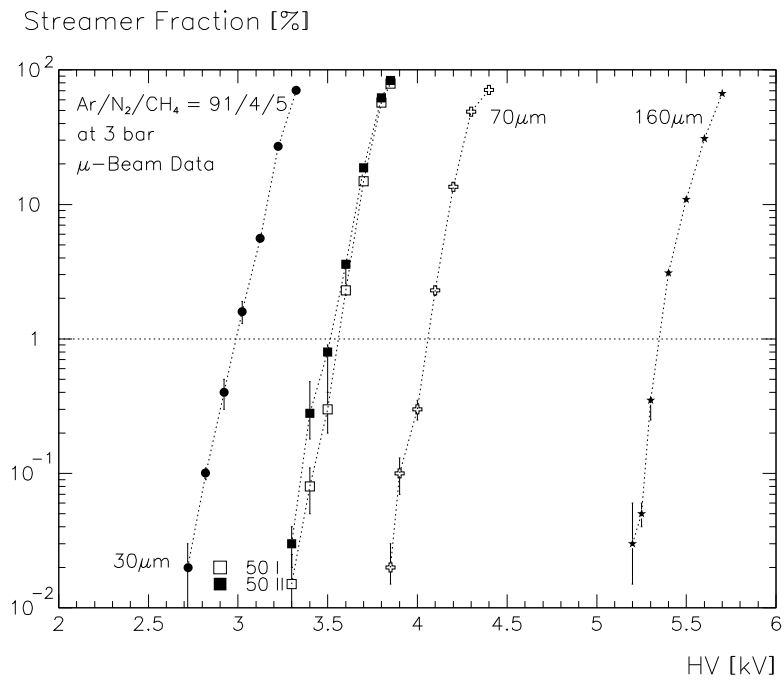
Figure 18: Limited streamer fraction versus HV, Ar:N$_2$:CH$_4$=91:4:5 at 3 bar, μ-beam data.
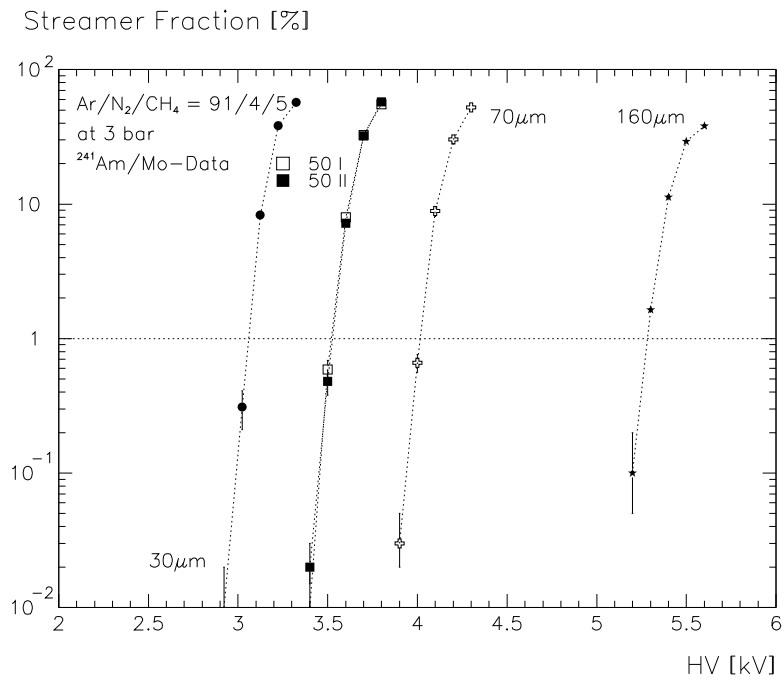
Figure 19: Limited streamer fraction versus HV, Ar:N$_2$:CH$_4$=91:4:5 at 3 bar, ^{241}Am/Mo data.

21
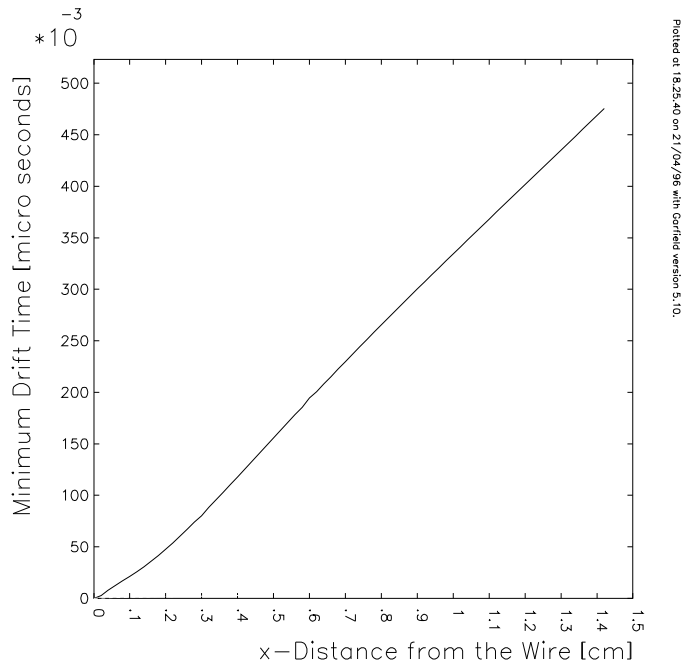
Figure 20: Garfield RT-simulation for Ar:N$_2$:CH$_4$=91:4:5 at 3.25 kV (gas gain 2 × 10^4), 50 μm wire, pressure = 3 bar, temperature = 300 K, magnetic field = 0 T.
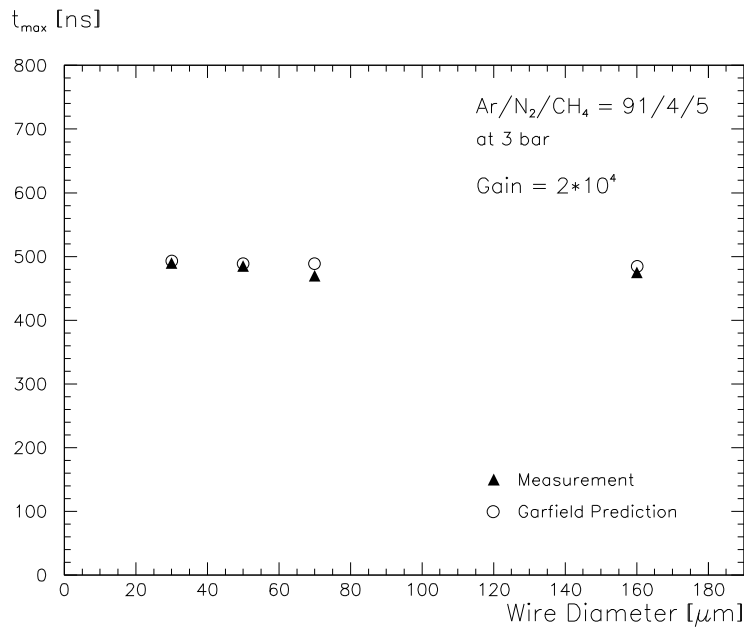
Figure 21: Maximum drift times versus wire diameter for Ar:N$_2$:CH$_4$=91:4:5 at 3 bar, gas gain 2 · 10^4.

22

7.2 Ar:CO_2:CH_4=92:5:3

Fig. 22 shows the gas gain for the muon data. For the Ar:CO_2:CH_4=92:5:3 gas no ^{241}Am data was taken. Fig. 23 compares the ^{55}Fe and beam measurements.

Table 8 lists the Diethorn parameters for the muon data. The 30, 70 and 160 μm wires give the same results, within the errors, but the 50 μm wire deviates by a factor of 2. The 50 μm showed the biggest deviations from the Garfield rt-relationship and possibly our simple scaling of the Garfield rt-relationship to match the maximum drift times was insufficiently accurate, leading to the wrong correction factor for the charge extrapolation.

Fig. 24 shows the limited streamer fraction for muons. Fig. 25 shows a comparison between the beam and ^{55}Fe data for the 50 μm wire. For a gain of 2×10^4 the streamer rate is well below 1%, for all wire diameters. Due to the above mentioned difficulties in the gain measurement, the results for the 50 μm wire could have a large systematic error. The charge contained in a single streamer is small (3–5 times the proportional charge). Fig. 26 and fig. 27 show the corresponding plots for the HV dependence of the limited streamer rates.

The gas mixture Ar:CO_2:CH_4=92:5:3 has a very nonlinear rt-relationship, see fig. 28. Garfield predictions of the maximum drift time are around 500 ns. Fig. 29 shows the dependence of the maximum drift time, taken from the first hit TDC spectra, on the wire diameter. As expected for a nonlinear gas, the maximum drift time is a strong function of wire diameter. The observed maximum drift times were inconsistent. During the measurement period 3 bottles of premixed gas were used. For the first bottle the measured maximum drift times were up to 300 ns longer than the Garfield predictions; for the second and third bottle, they were 100 ns longer.

The dependence of the drift times on the HV follows Garfield, except for the 160 μm wire. The measurements suggest that the Ar:CO_2:CH_4=92:5:3 gas is affected strongly by contaminations; temperature changes were uncorrelated with the measured drift times, and the gas pressure was constant. By adding 0.2-0.5% of water in the Garfield simulation it is possible to reproduce the observed drift times for the first bottle. Nevertheless the drift time behaviour of the 160 μm tube cannot be explained by merely adding water. The observed variations are enormous and would require an extremely careful control of gas impurities to achieve the stability needed at ATLAS.

After-pulsing poses no problem for the Ar:CO_2:CH_4=92:5:3 mixture. The gas gain at which the 1% level is reached is well above the (proposed) working point of 2×10^4, see table 7.

Wire diam. [μm]	High Voltage [V]	Gas Gain [10^4]
30	3100 ± 20	10.0 ± 1.0
50	3700 ± 20	11.0 ± 1.0
70	3900 ± 20	6.0 ± 0.5
160	5000 ± 20	6.5 ± 0.5

Table 7: High voltages and gas gains for 1% after-pulsing, Ar:CO_2:CH_4=92:5:3 at 3 bar.
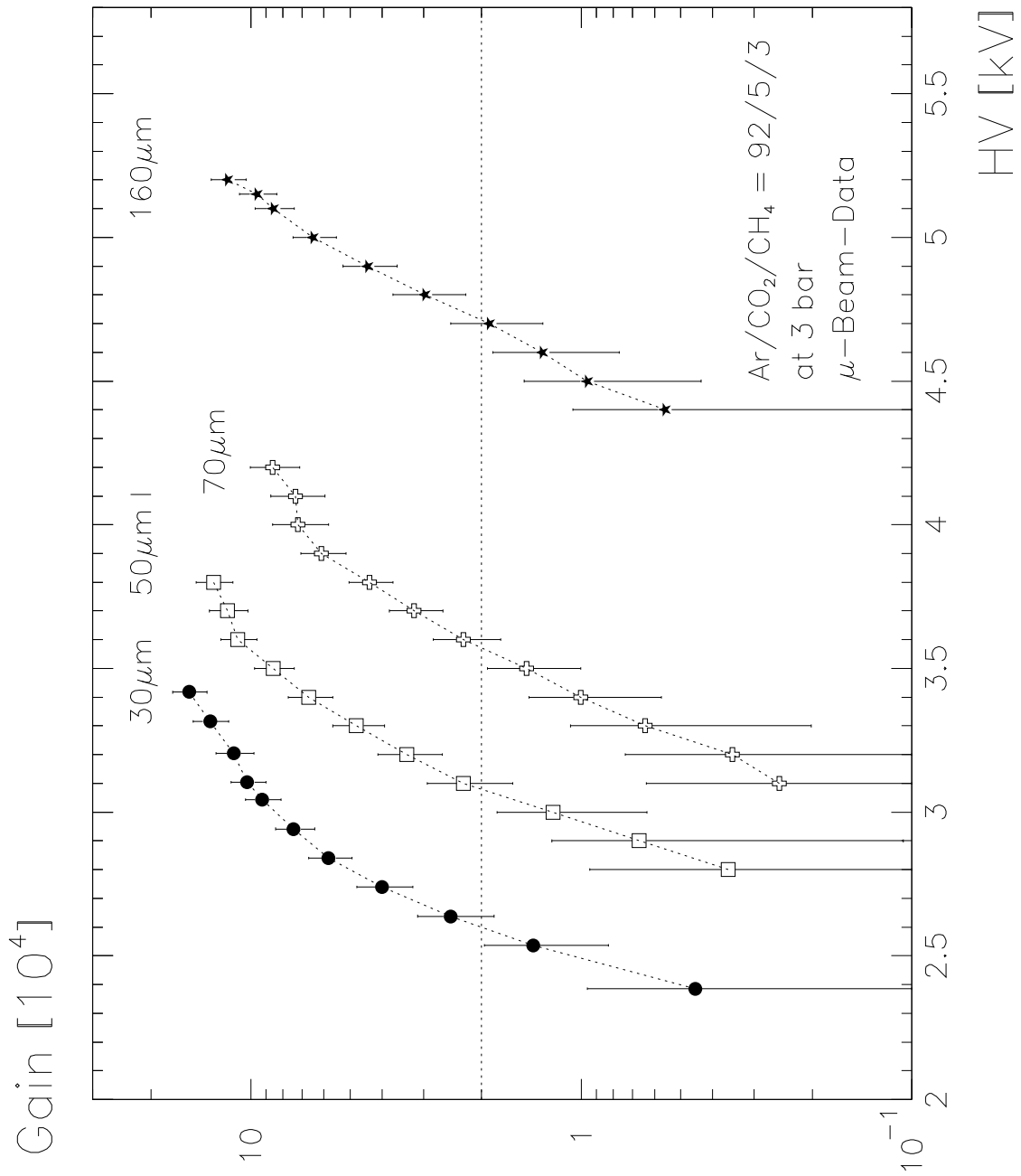
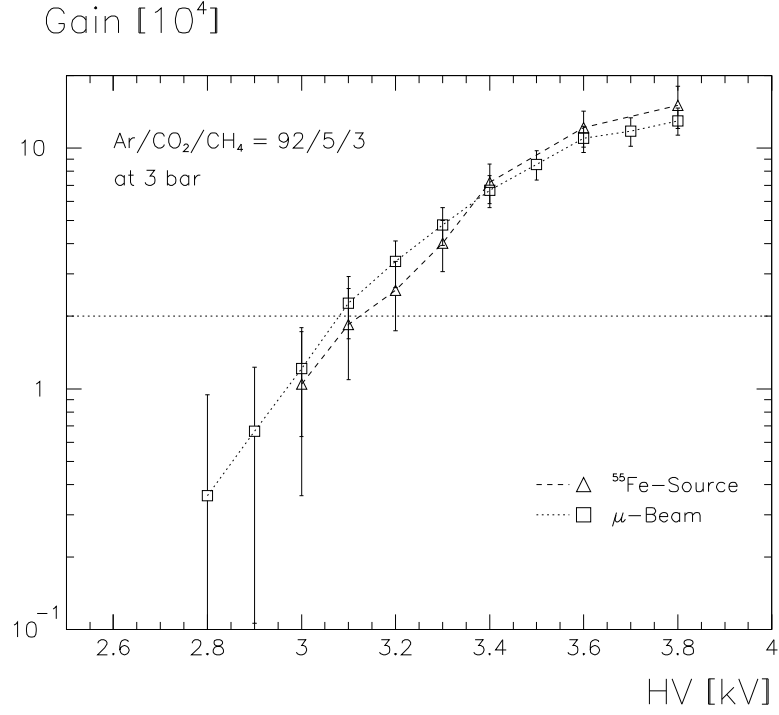**Figure 22:** Gas gain versus HV, Ar:CO$_2$:CH$_4$=92:5:3 at 3 bar, μ-beam data.

Figure 23: Gas gain versus HV, Ar:CO$_2$:CH$_4$=92:5:3 at 3 bar, 50 μm wire.

Wire diam. [μm]	$\Delta\Phi$ [V]	E_{min}(3 bar) [kV/cm]	E_{min}(1 bar) [kV/cm]
30	71 $\pm$ 14	17 $\pm$ 9 $\pm$ 9	6 $\pm$ 3 $\pm$ 3
50 I	36 $\pm$ 1	67 $\pm$ 1 $\pm$ 2	22 $\pm$ 0 $\pm$ 1
70	79 $\pm$ 6	25 $\pm$ 4 $\pm$ 5	8 $\pm$ 1 $\pm$ 2
160	70 $\pm$ 3	37 $\pm$ 2 $\pm$ 3	12 $\pm$ 1 $\pm$ 1

Table 8: Diethorn parameters for Ar:CO$_2$:CH$_4$=92:5:3, μ-beam data.
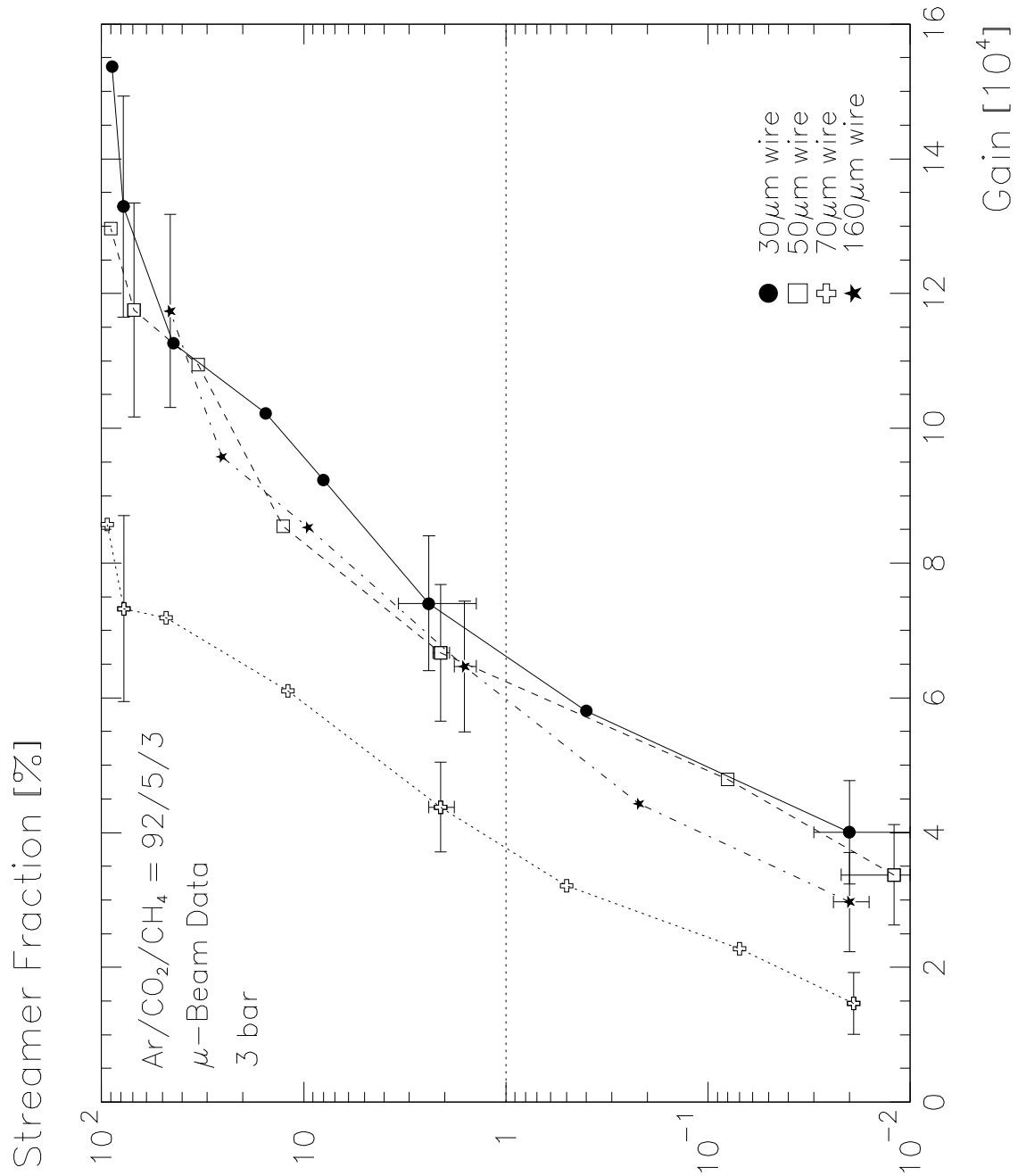
Figure 24: Limited streamer fraction versus gas gain, $Ar:CO_2:CH_4=92:5:3$ at 3 bar, μ-beam data. Only a representative sample of error bars is shown.
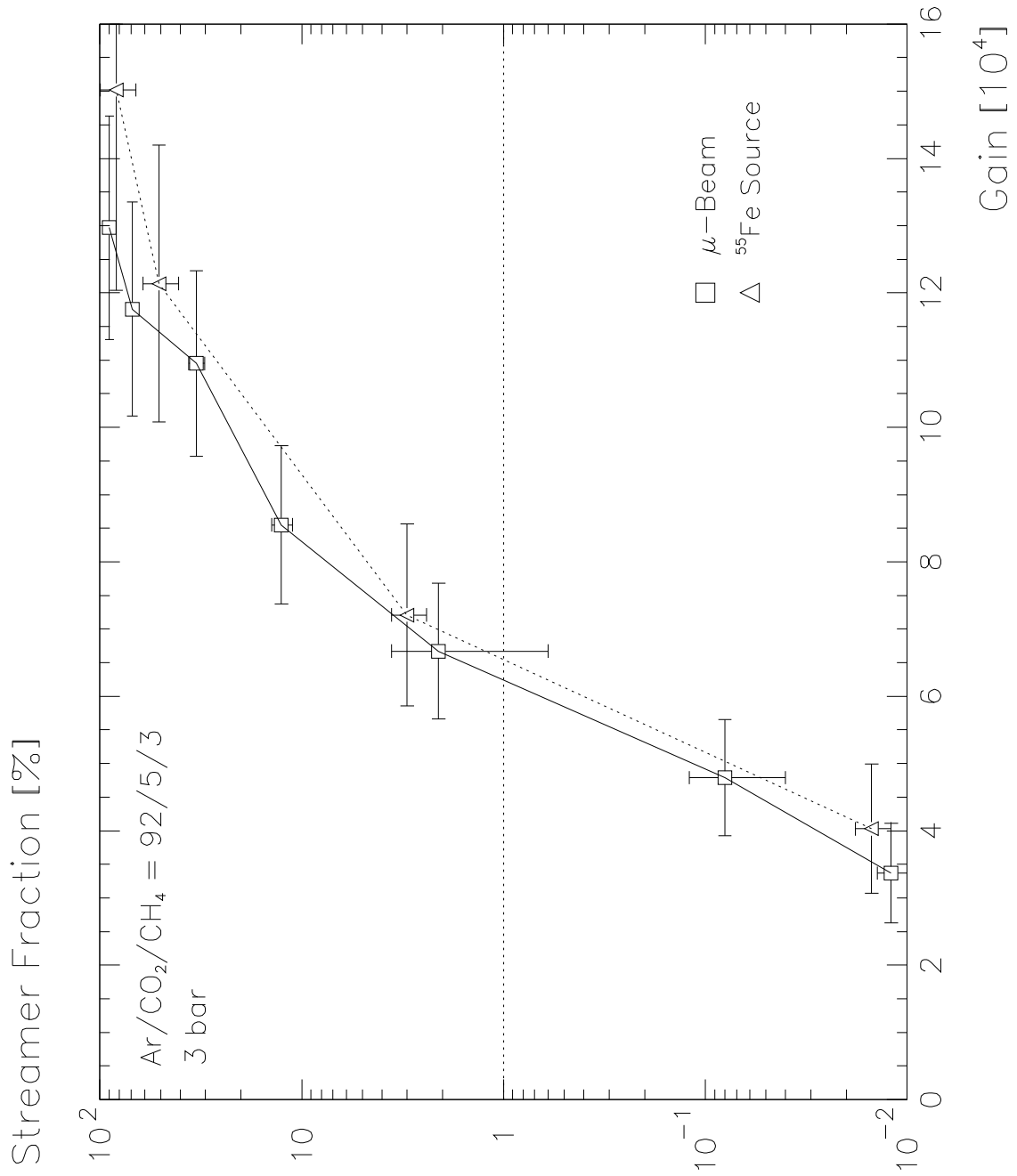
Figure 25: Comparison of the limited streamer fraction versus gas gain, $Ar:CO_2:CH_4=92:5:3$ at 3 bar, 50 μm wire.
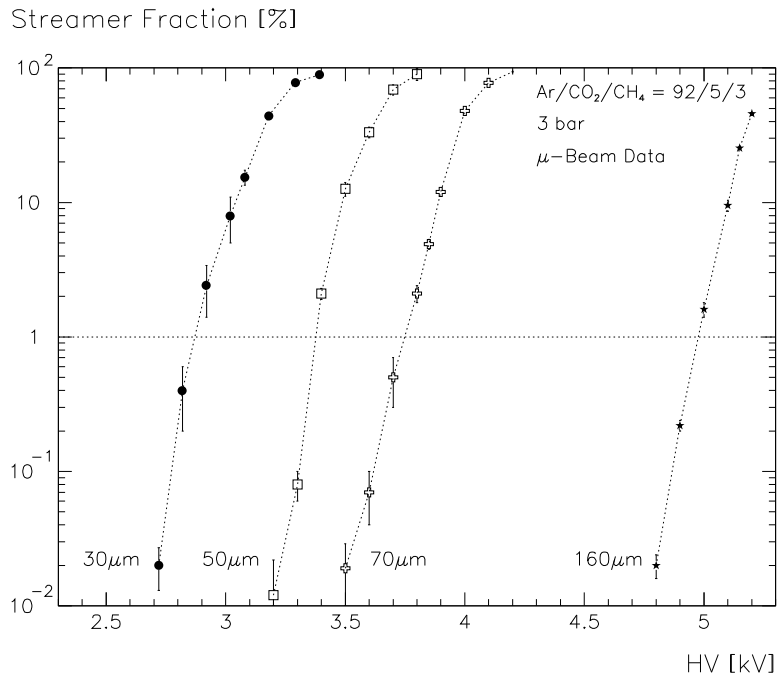
Streamer Fraction [%]

Figure 26: Limited streamer fraction versus HV, Ar:CO_2:CH_4=92:5:3 at 3 bar, μ beam data.
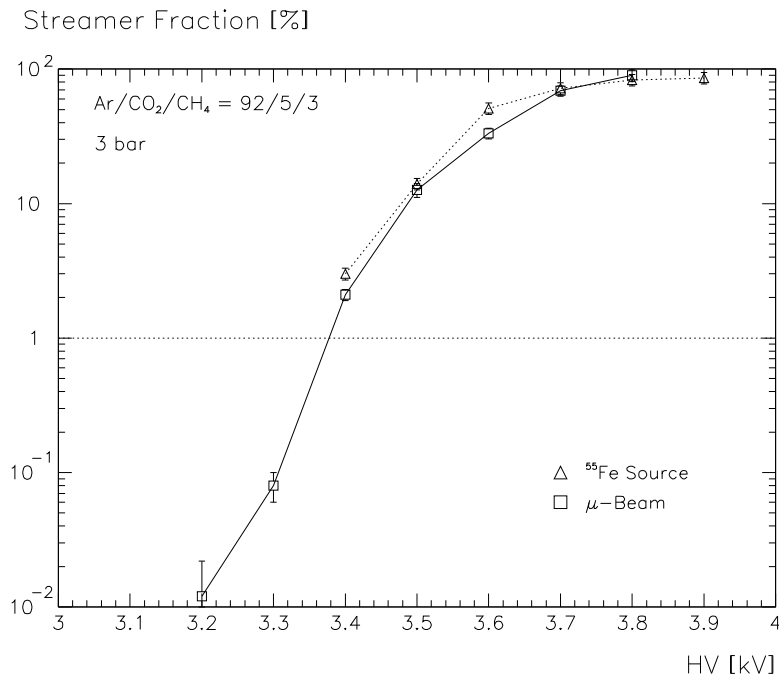
Streamer Fraction [%]

Figure 27: Comparison of the limited streamer fraction versus HV, Ar:CO_2:CH_4=92:5:3 at 3 bar, 50 μm wire.
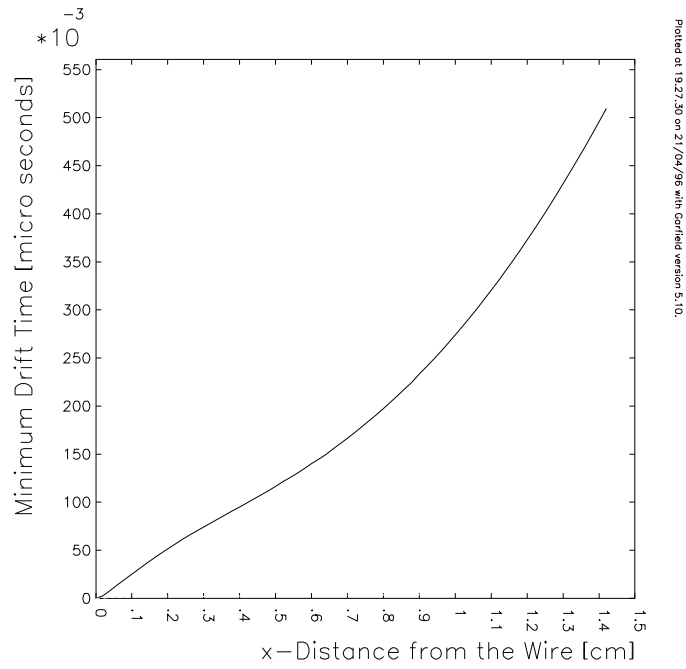
Figure 28: Garfield RT-simulation for Ar:CO_2:CH_4=92:5:3 at 3.08 kV (gas gain 2×10^4), 50 μm wire, pressure = 3 bar, temperature = 300 K, magnetic field = 0 T.
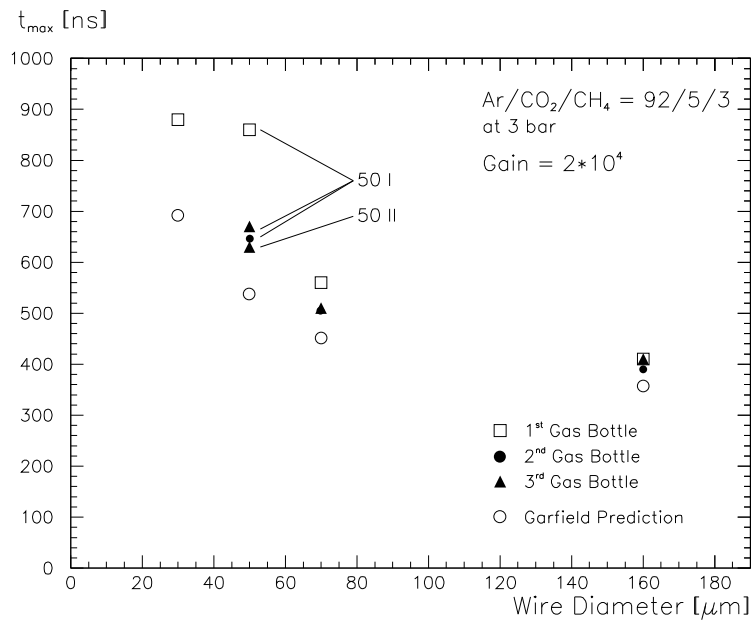
Figure 29: Maximum drift times versus wire diameter for Ar:CO_2:CH_4=92:5:3 at 3 bar, gas gain $2 \cdot 10^4$.

7.3 Ar:CO$_2$:CH$_4$=93:4:3

Fig. 30 and fig. 31 show the gas gain for μ-beam data and ^{241}Am data. The comparison of the gas gain measurements for beam and gamma-source data, fig. 32, shows the same systematic effect as for the Ar:N$_2$:CH$_4$=91:4:5 gas.

The Diethorn parameters are given in Tables 10, 11 and 12. Again the source measurements give different values from the beam measurements, but within a group the data is consistent.

Fig. 33 and fig. 34 give the results for the limited streamer fraction dependence on the gas gain. No ^{241}Am measurement was made because the streamer pulses coincide with the 60 keV peak of the source. Of all gases studied the Ar:CO$_2$:CH$_4$=93:4:3 mixture shows the highest streamer rates, but the charge contained in a single limited streamer pulse is small (3–5 times the proportional charge). Fig. 35 and fig. 36 show the dependence of the limited streamer fraction on the HV.

This gas is a derivative of the Ar:CO$_2$:CH$_4$=92:5:3 gas. The amount of CO$_2$ was reduced by 1% to achieve a (slightly) more linear rt-relationship (fig. 37) and to make the gas faster. The reduction of CO$_2$ makes the mixture also a little less prone to effects of contaminations.

All observed maximum drift times are slower than the Garfield predictions, with deviations up to 150 ns. Apart from the different maximum drift time values the dependence on the HV follows the Garfield prediction. Fig. 38 shows the dependence of the maximum drift times on the wire diameter for a gas gain of $2 \cdot 10^4$. As expected for a nonlinear gas, the drift times become smaller with increasing wire diameter.

After-pulsing poses no problem with this gas. The level of 1% after-pulsing is only reached at high gains, around $8 \cdot 10^4$, see Table 9.

Wire diam. [μm]	High Voltage [V]	Gas Gain [10^4]
30	3200 ± 20	9.0 ± 0.9
50	3600 ± 20	8.5 ± 0.9
70	3900 ± 20	7.5 ± 0.8
160	4900 ± 20	8.0 ± 0.8

Table 9: High voltages and gas gains for 1% after-pulsing, Ar:CO$_2$:CH$_4$=93:4:3 at 3 bar.
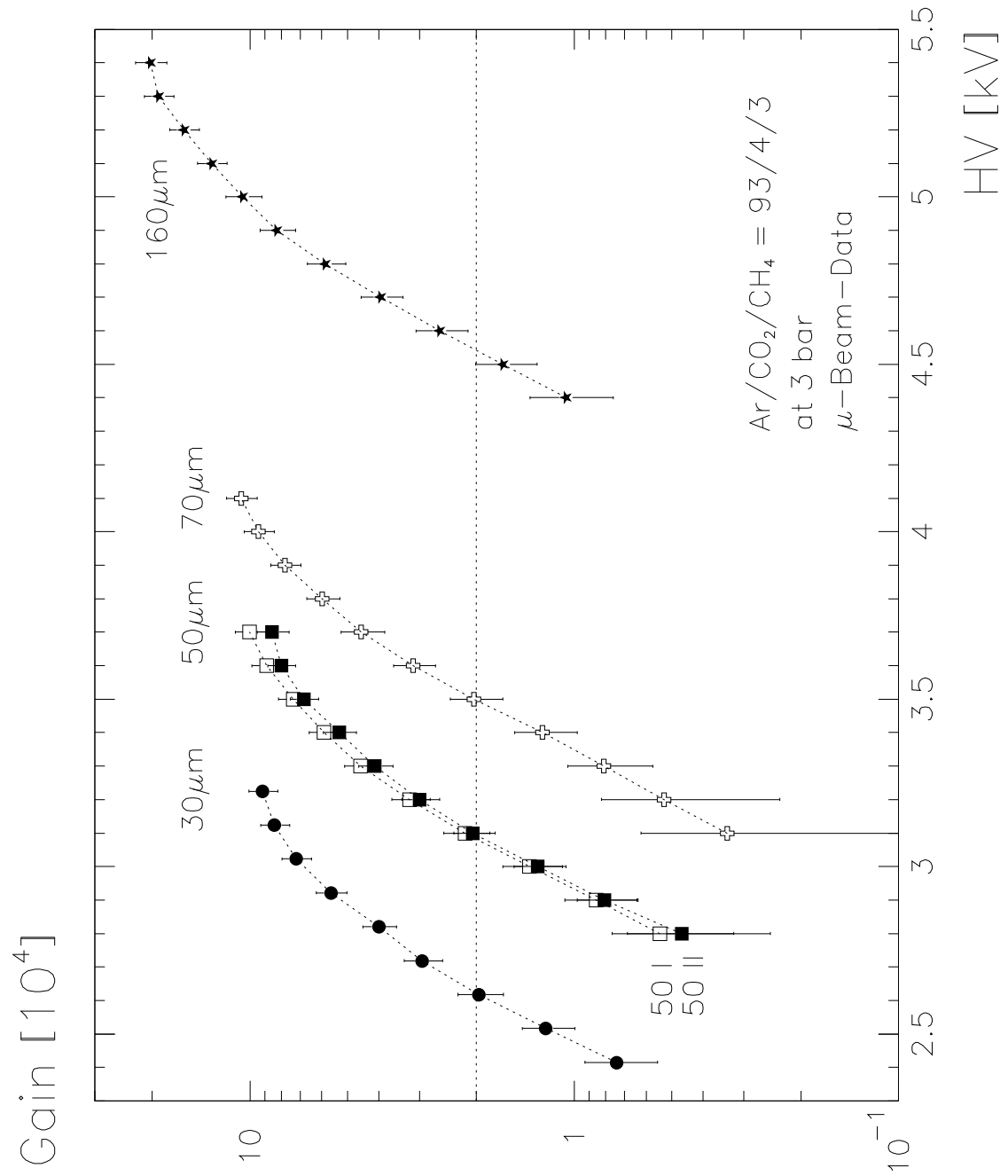
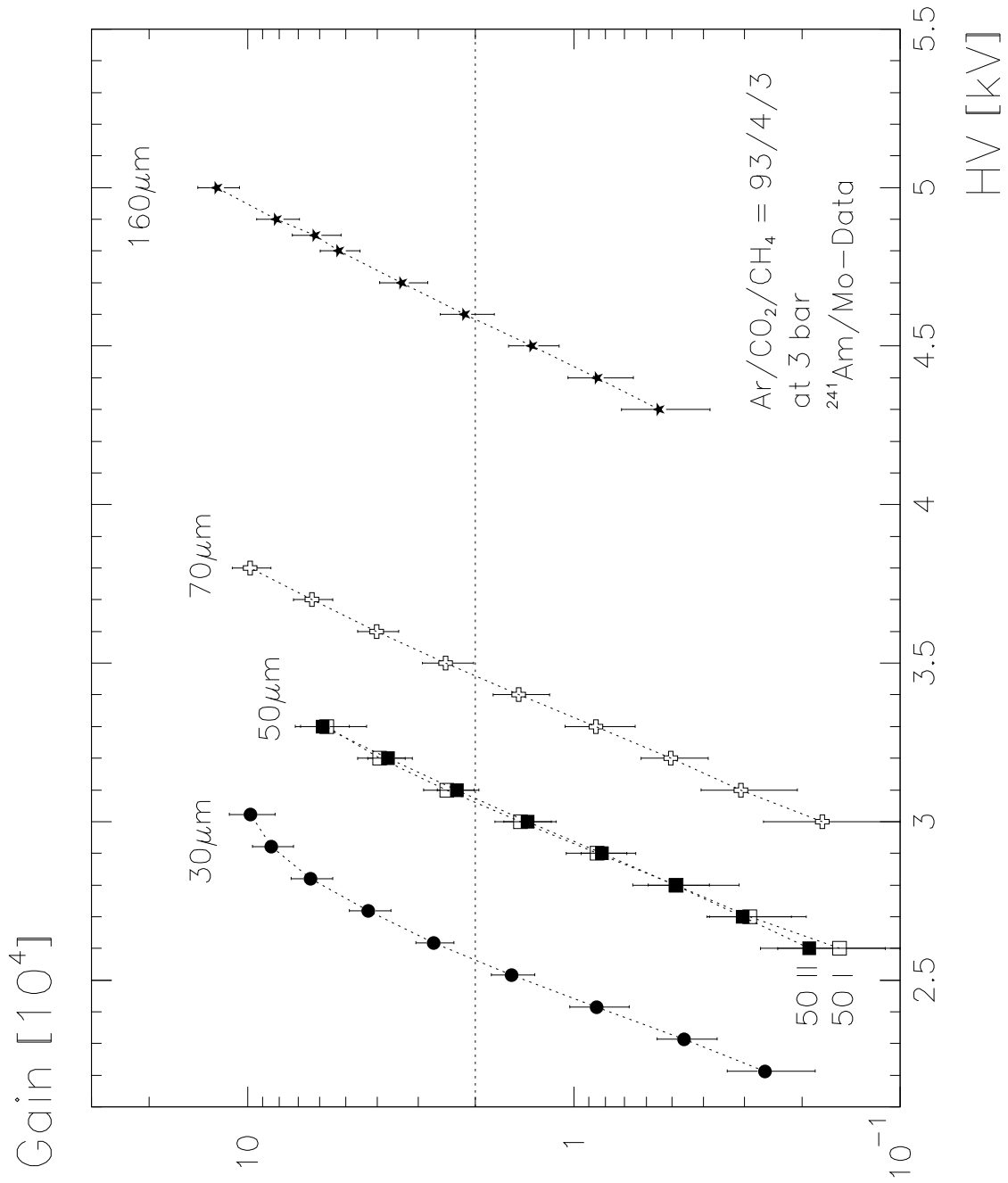**Figure 30:** Gas gain versus HV, Ar:CO$_2$:CH$_4$=93:4:3 at 3 bar, μ-beam data.

Figure 31: Gas gain versus HV, $Ar:CO_2:CH_4=93:4:3$ at 3 bar, $^{241}Am/Mo$ data.
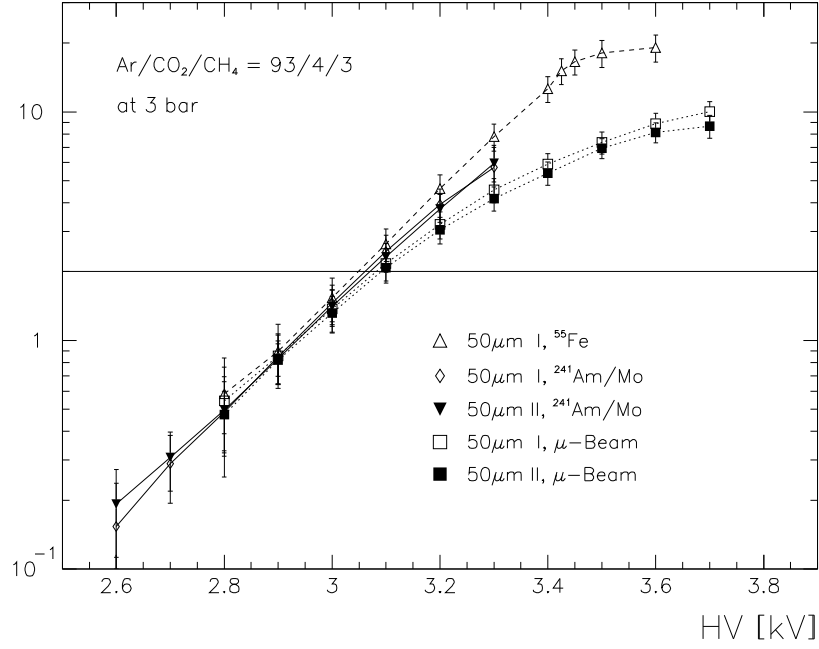
Figure 32: Comparison of the gas gain measurements, $Ar:CO_2:CH_4=93:4:3$ at 3 bar, 50 μm wire.

Wire diam. [μm]	$\Delta\Phi$ [V]	E_{min}(3 bar) [kV/cm]	E_{min}(1 bar) [kV/cm]
30	77 ± 5	$14 \pm 2 \pm 10$	$4.7 \pm 0.6 \pm 3.5$
50 I	74 ± 1	$22 \pm 1 \pm 5$	$7.3 \pm 0.3 \pm 1.7$
50 II	72 ± 10	$23 \pm 7 \pm 4$	$7.8 \pm 2.3 \pm 1.2$
70	72 ± 5	$28 \pm 1 \pm 7$	$9.3 \pm 0.1 \pm 2.5$
160	74 ± 4	$33 \pm 2 \pm 6$	$10.9 \pm 0.7 \pm 2.1$

Table 10: Diethorn parameters for $Ar:CO_2:CH_4=93:4:3$, μ-beam data.

Wire diam. [μm]	$\Delta\Phi$ [V]	E_{min}(3 bar) [kV/cm]	E_{min}(1 bar) [kV/cm]
30	44 ± 1	$44 \pm 2 \pm 7$	$15 \pm 1 \pm 2$
50 I	47 ± 1	$48 \pm 1 \pm 9$	$16 \pm 0 \pm 3$
50 II	51 ± 1	$42 \pm 1 \pm 11$	$14 \pm 0 \pm 4$
70	45 ± 1	$50 \pm 1 \pm 7$	$18 \pm 0 \pm 2$
160	54 ± 1	$46 \pm 1 \pm 5$	$15 \pm 0 \pm 2$

Table 11: Diethorn parameters for $Ar:CO_2:CH_4=93:4:3$, [241]Am/Mo data.

Wire diam. [μm]	$\Delta\Phi$ [V]	E_{min}(3 bar) [kV/cm]	E_{min}(1 bar) [kV/cm]
50 I	51 ± 1	$42 \pm 1 \pm 2$	$14 \pm 0 \pm 1$

Table 12: Diethorn parameters for $Ar:CO_2:CH_4=93:4:3$, [55]Fe data.
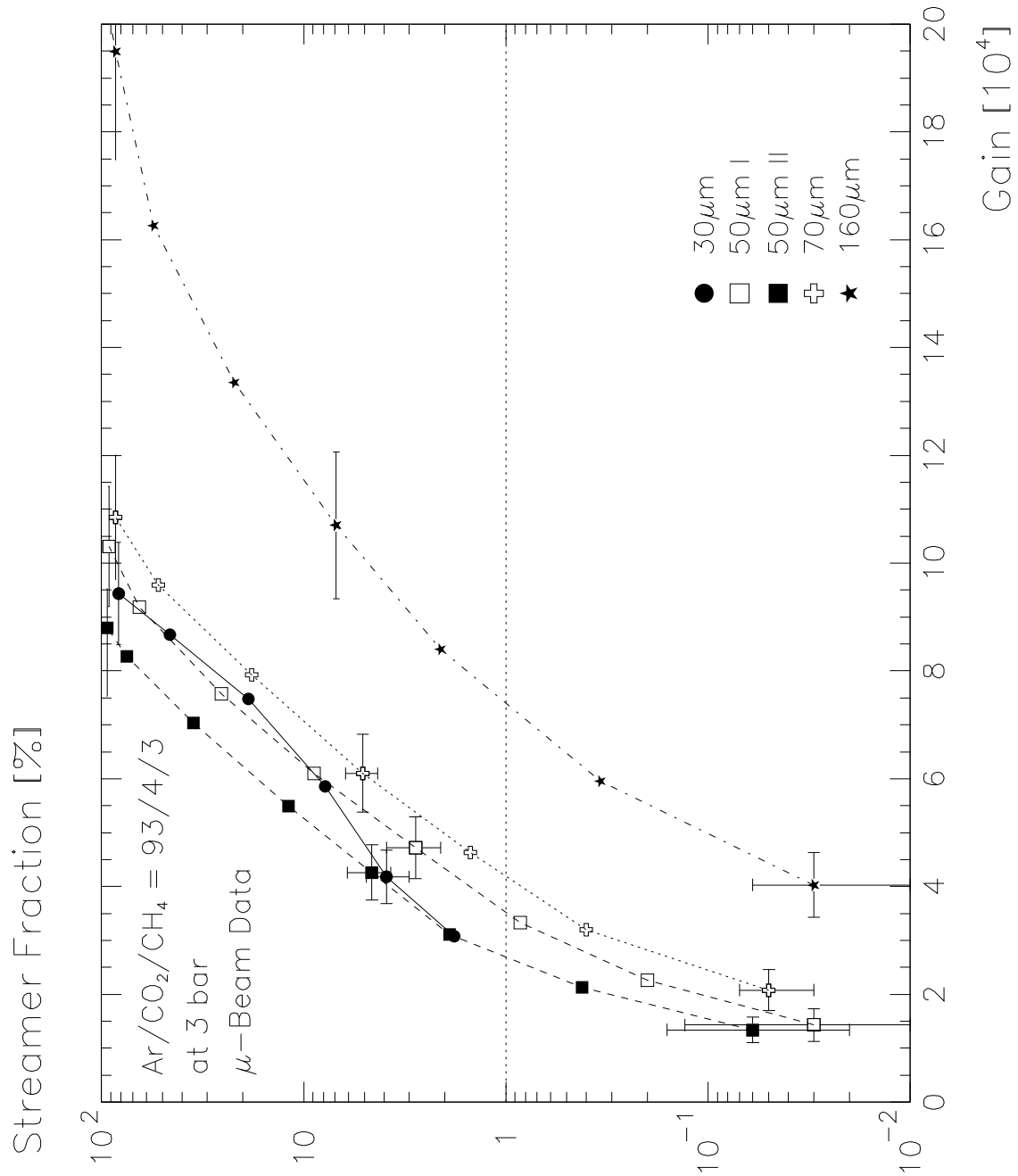
Figure 33: Limited streamer fraction versus gas gain, Ar:CO$_2$:CH$_4$=93:4:3 at 3 bar, μ-beam data. Only a representative sample of error bars is shown.
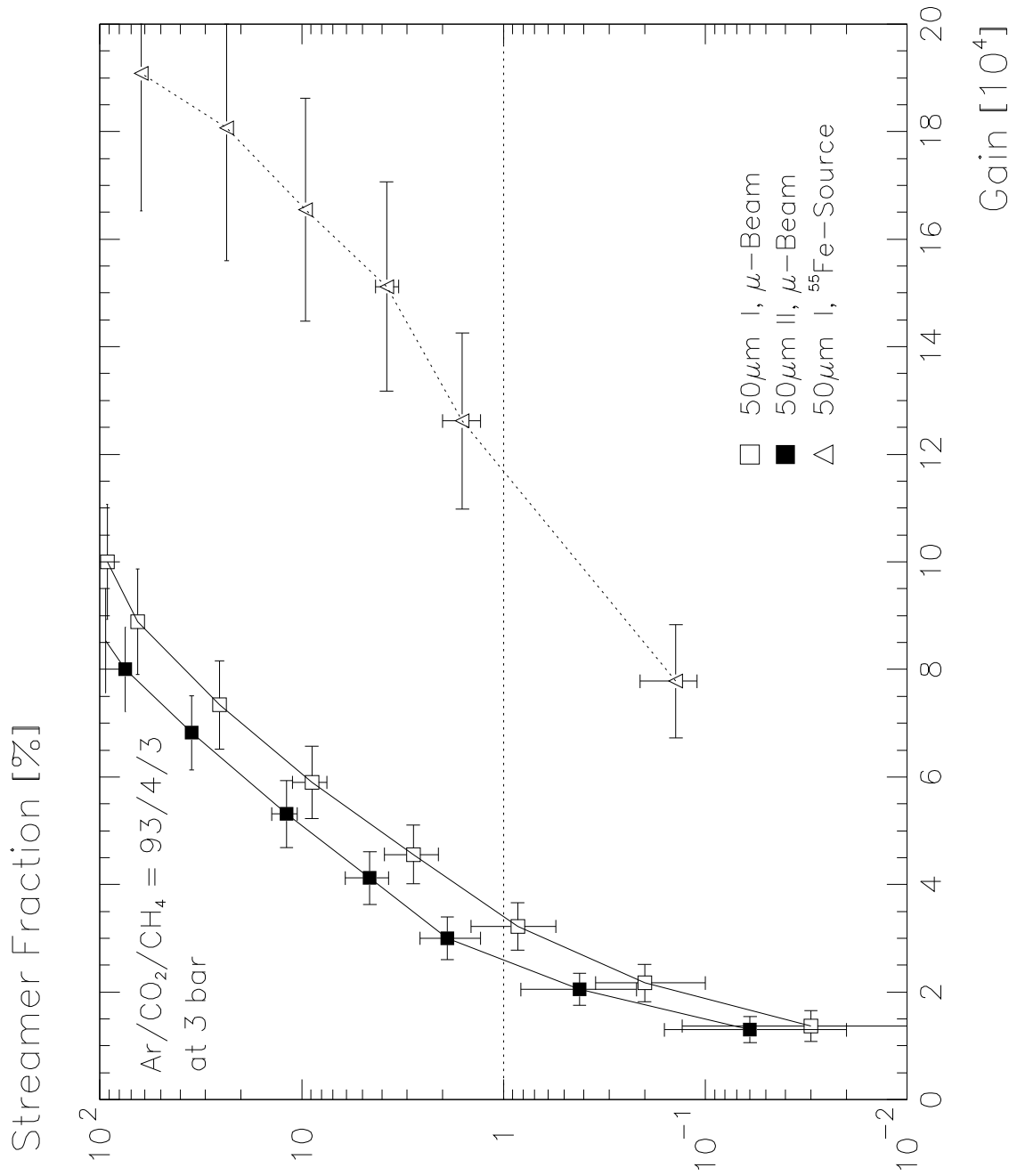
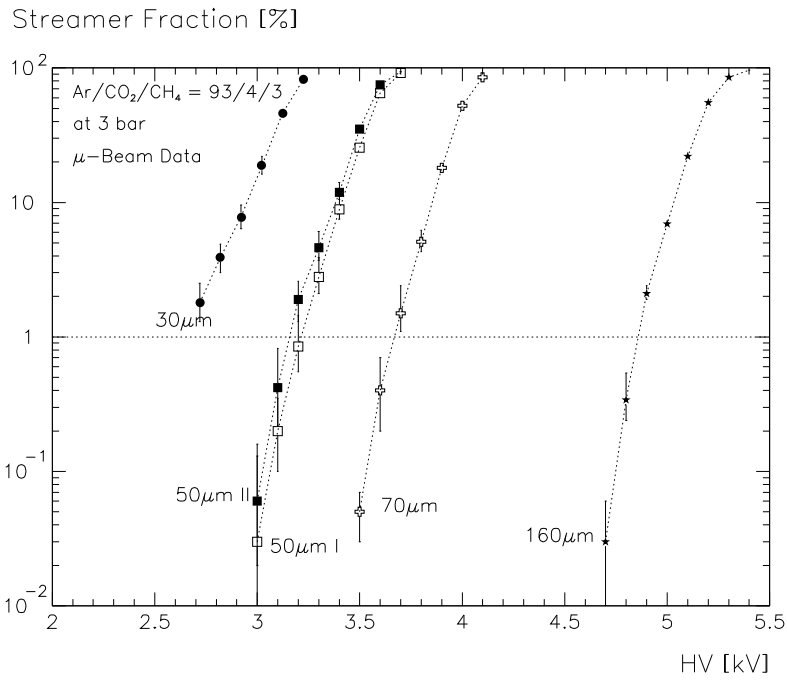**Figure 34:** Comparison of the limited streamer fraction versus gas gain, Ar:CO$_2$:CH$_4$=93:4:3 at 3 bar, 50 μm wire.

Figure 35: Limited streamer fraction versus HV, Ar:CO_2:CH_4=93:4:3 at 3 bar, μ-beam data.
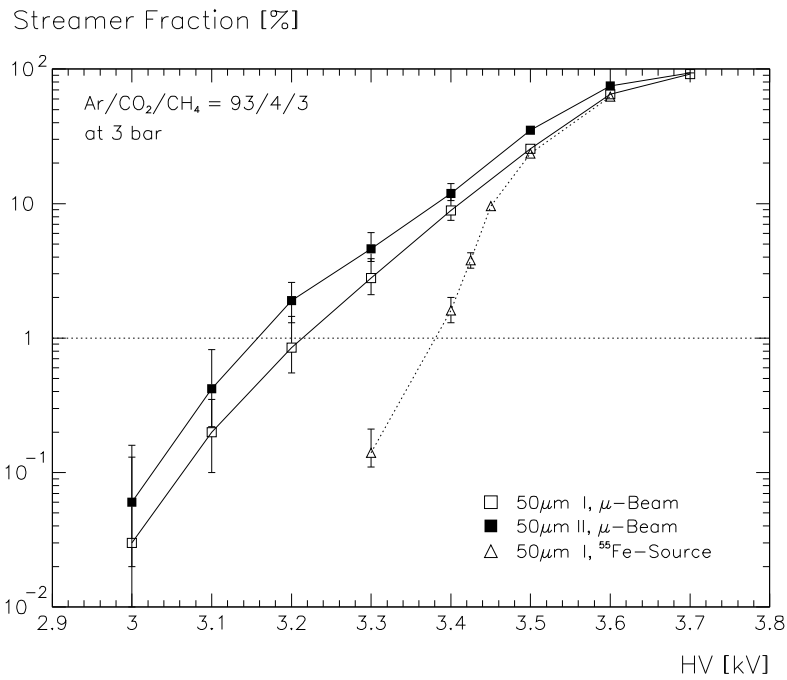
Figure 36: Comparison of the limited streamer rates versus HV, Ar:CO_2:CH_4=93:4:3 at 3 bar, 50 μm wire.
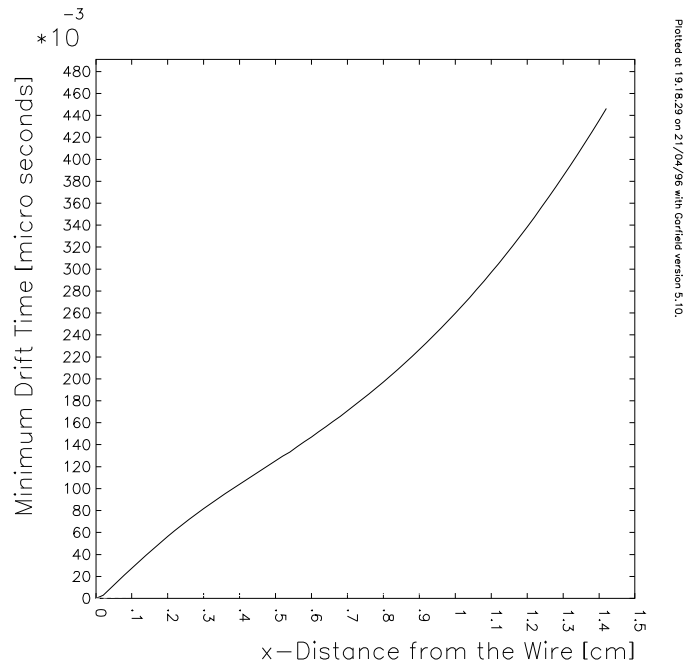
Figure 37: Garfield RT-simulation for Ar:CO$_2$:CH$_4$=93:4:3 at 3.09 kV (gas gain 2×10^4), 50 μm wire, pressure = 3 bar, temperature = 300 K, magnetic field = 0 T.
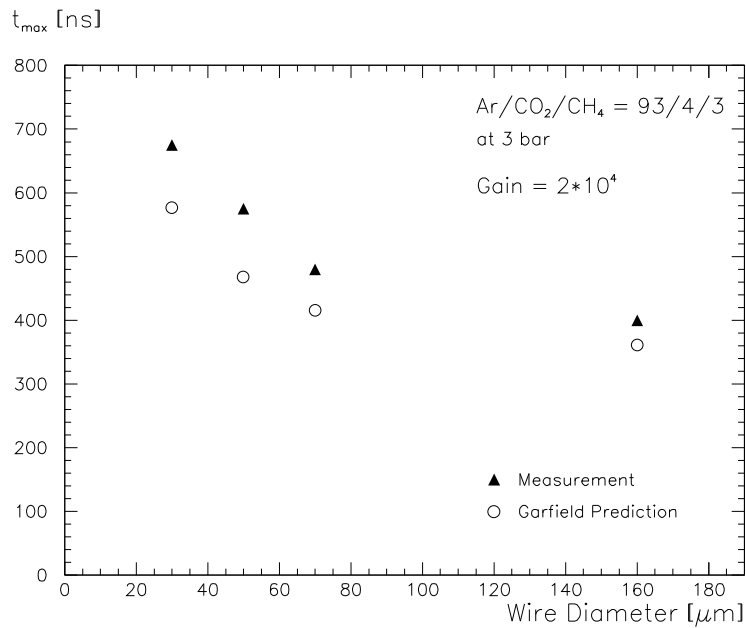
Figure 38: Maximum drift times versus wire diameter for Ar:CO$_2$:CH$_4$=93:4:3 at 3 bar, gas gain $2 \cdot 10^4$.

7.4 $Ar:N_2:CO_2:CF_4=95:2:2:1$

Fig. 39 shows the gas gain for μ-beam data, fig. 40 for ^{241}Am data. For the 50 μm tubes fig. 41 compares the beam, ^{241}Am and ^{55}Fe measurements. Again, the slopes for the beam measurements are smaller than for the source data.

Tables 14, 15 and 16 list the Diethorn parameters for this gas. While the source measurements are consistent, the beam data shows a large spread.

Fig. 42 and fig. 43 give the limited streamer rates for beam and ^{241}Am data, and fig. 44 shows the comparison for the 50 μm wires, including the ^{55}Fe data. At a gain of 2×10^4 the streamer rate is well below the 1% level for all measurements and wire diameters. We were unable to measure the charge contained in the streamer signals because of pre amp and ADC saturation. As for the $Ar:N_2:CH_4=91:4:5$ mixture, we can only give a lower limit of around 10 times the charge of a proportional signal. Fig. 45 and fig. 46 show the dependence of the the limited streamer fraction on the HV.

The four component mixture $Ar:N_2:CO_2:CF_4=95:2:2:1$ is the only gas mixture studied that contains no flammable components. It is linear at a magnetic field of 0.6 T, but exhibits a small nonlinearity under our operating conditions of zero magnetic field (fig 47). The Garfield maximum drift time predictions are in reasonable agreement with the observed ones (deviations were smaller than 10%), the Garfield prediction being too fast in all cases. The influence of the wire diameter on the maximum drift time is rather strong, with the 30 μm tube 150 ns slower than the 160 μm tube (fig. 48).

This mixture shows the highest after-pulsing rates of all the gases we studied. Although the rate is smaller than 1% at a gas gain of $2 \cdot 10^4$, it is near this level. Some after-pulses could be observed on the oscilloscope at this gain. Table 13 lists the HV and gas gain for the 1% level for all wire diameters.

The reason for the high after-pulsing rates might be that the quenching ability of CF_4 is too weak. In the 1996 test beam a similar mixture with twice the amount of quencher, $Ar:N_2:CO_2:CF_4=90:4:4:2$, may be studied.

Wire diam. $[\mu m]$	High Voltage [V]	Gas Gain $[10^4]$
30	2850 ± 20	3.5 ± 0.4
50	3400 ± 20	3.1 ± 0.3
70	3900 ± 20	2.8 ± 0.3
160	5200 ± 20	3.2 ± 0.3

Table 13: High voltages and gas gains for 1% after-pulsing, $Ar:CO_2:N_2:CF_4=95:2:2:1$ at 3 bar.
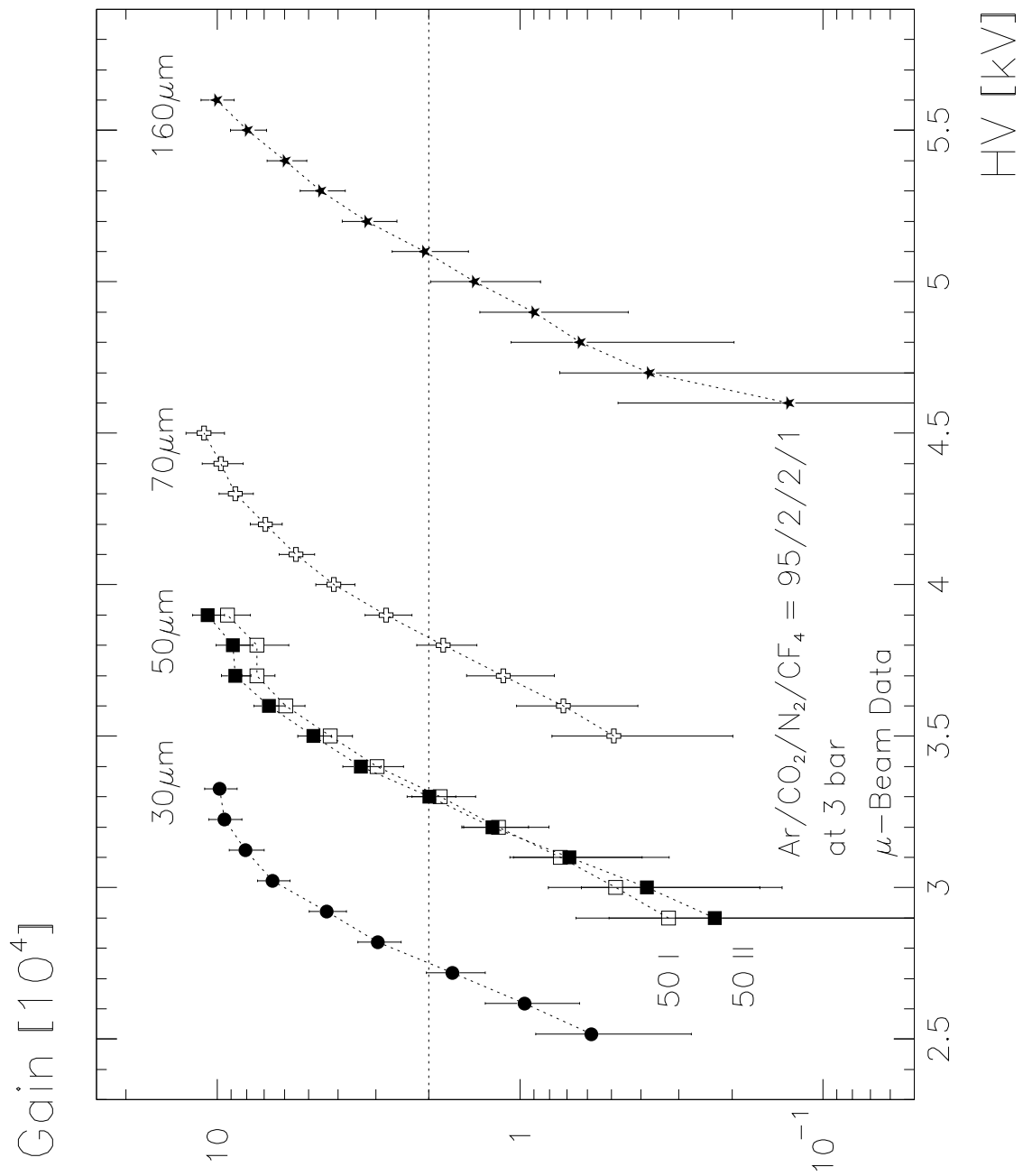
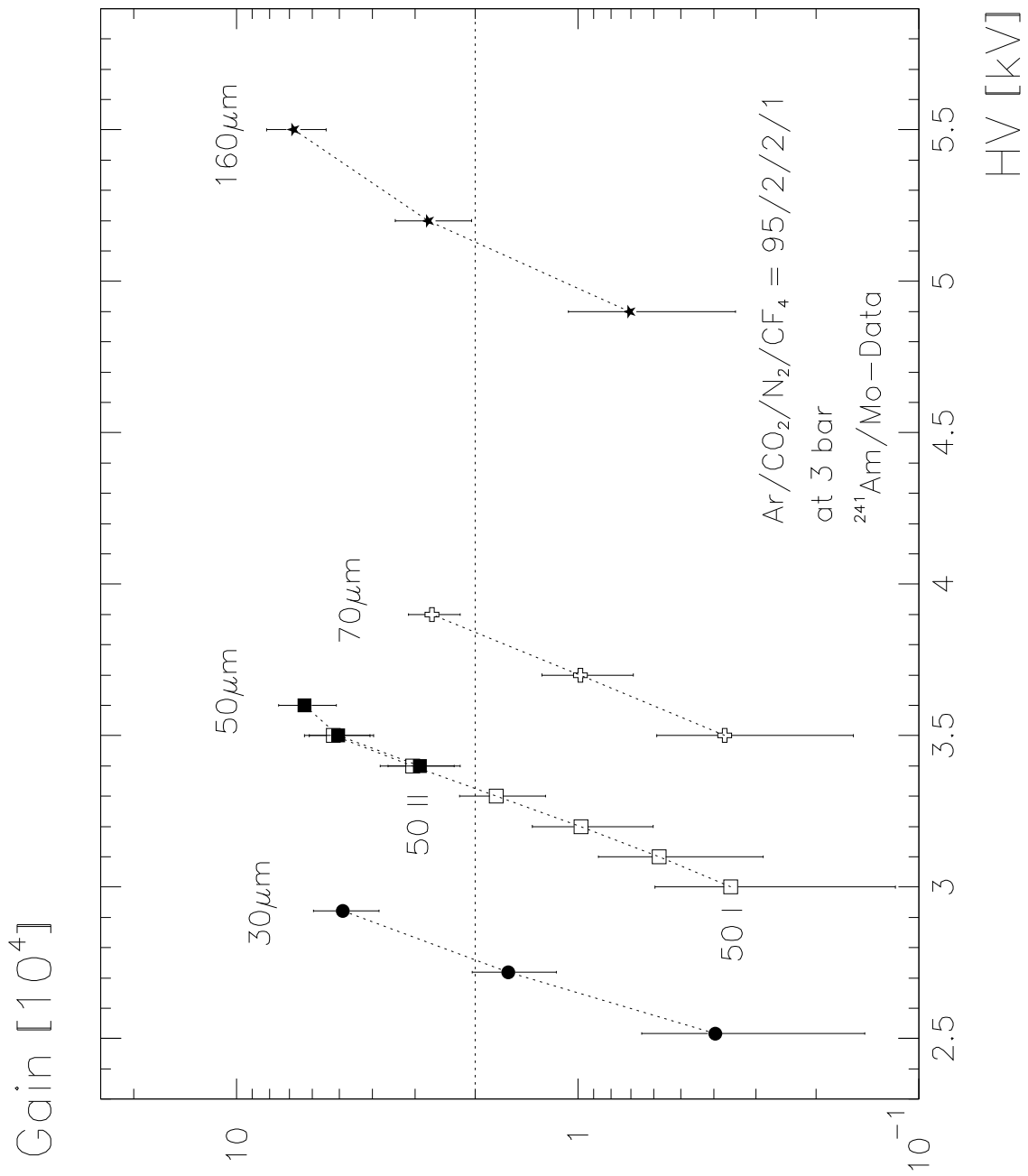**Figure 39:** Gas gain versus HV, $Ar:N_2:CO_2:CF_4=95:2:2:1$ at 3 bar, μ-beam data.

Figure 40: Gas gain versus HV, Ar:N$_2$:CO$_2$:CF$_4$=95:2:2:1 at 3 bar, ^{241}Am/Mo.
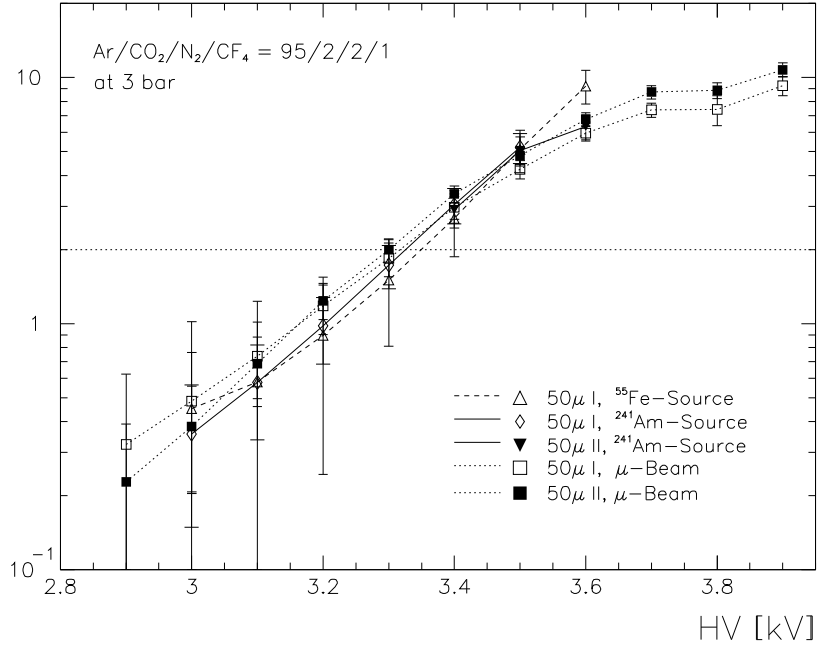
Figure 41: Comparison of the gas gain measurements, $Ar:CO_2:N_2:CF_4=95:2:2:1$ at 3 bar, 50 μm wires.

Wire diam. [μm]	$\Delta\Phi$ [V]	E_{min}(3 bar) [kV/cm]	E_{min}(1 bar) [kV/cm]
30	54 ± 2	$39 \pm 2 \pm 4$	$13 \pm 1 \pm 1$
50 I	73 ± 3	$28 \pm 2 \pm 4$	$9 \pm 1 \pm 1$
50 II	41 ± 3	$66 \pm 5 \pm 2$	$22 \pm 2 \pm 1$
70	62 ± 4	$45 \pm 4 \pm 4$	$15 \pm 1 \pm 1$
160	65 ± 23	$47 \pm 15 \pm 6$	$16 \pm 5 \pm 2$

Table 14: Diethorn parameters for $Ar:CO_2:N_2:CF_4=95:2:2:1$, μ-beam data.

Wire diam. [μm]	$\Delta\Phi$ [V]	E_{min}(3 bar) [kV/cm]	E_{min}(1 bar) [kV/cm]
30	39 ± 3	$66 \pm 3 \pm 5$	$22 \pm 1 \pm 2$
50 I	45 ± 2	$62 \pm 3 \pm 3$	$21 \pm 1 \pm 1$
50 II	44 ± 3	$63 \pm 4 \pm 10$	$21 \pm 1 \pm 3$
70	47 ± 1	$64 \pm 1 \pm 2$	$21 \pm 0 \pm 1$
160	50 ± 1	$59 \pm 1 \pm 3$	$20 \pm 0 \pm 1$

Table 15: Diethorn parameters for $Ar:CO_2:N_2:CF_4=95:2:2:1$, [241]Am/Mo data.

Wire diam. [μm]	$\Delta\Phi$ [V]	E_{min}(3 bar) [kV/cm]	E_{min}(1 bar) [kV/cm]
50 I	50 ± 5	$54 \pm 7 \pm 3$	$18 \pm 2 \pm 1$

Table 16: Diethorn parameters for $Ar:CO_2:N_2:CF_4=95:2:2:1$, [55]Fe data.
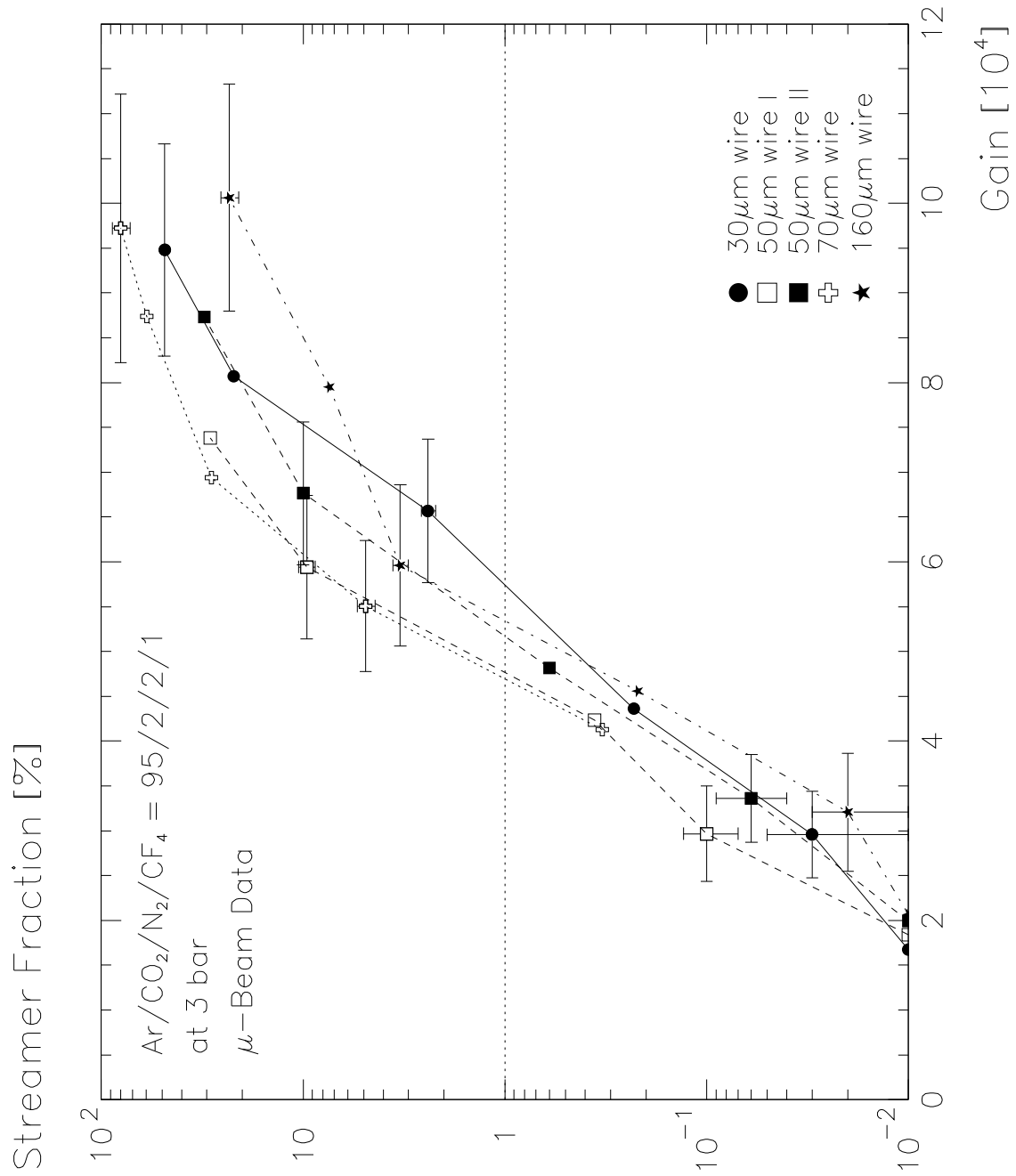
Figure 42: Limited streamer fraction versus gas gain, Ar:CO$_2$:N$_2$:CF$_4$=95:2:2:1 at 3 bar, μ-beam data. Only a representative sample of error bars is shown.
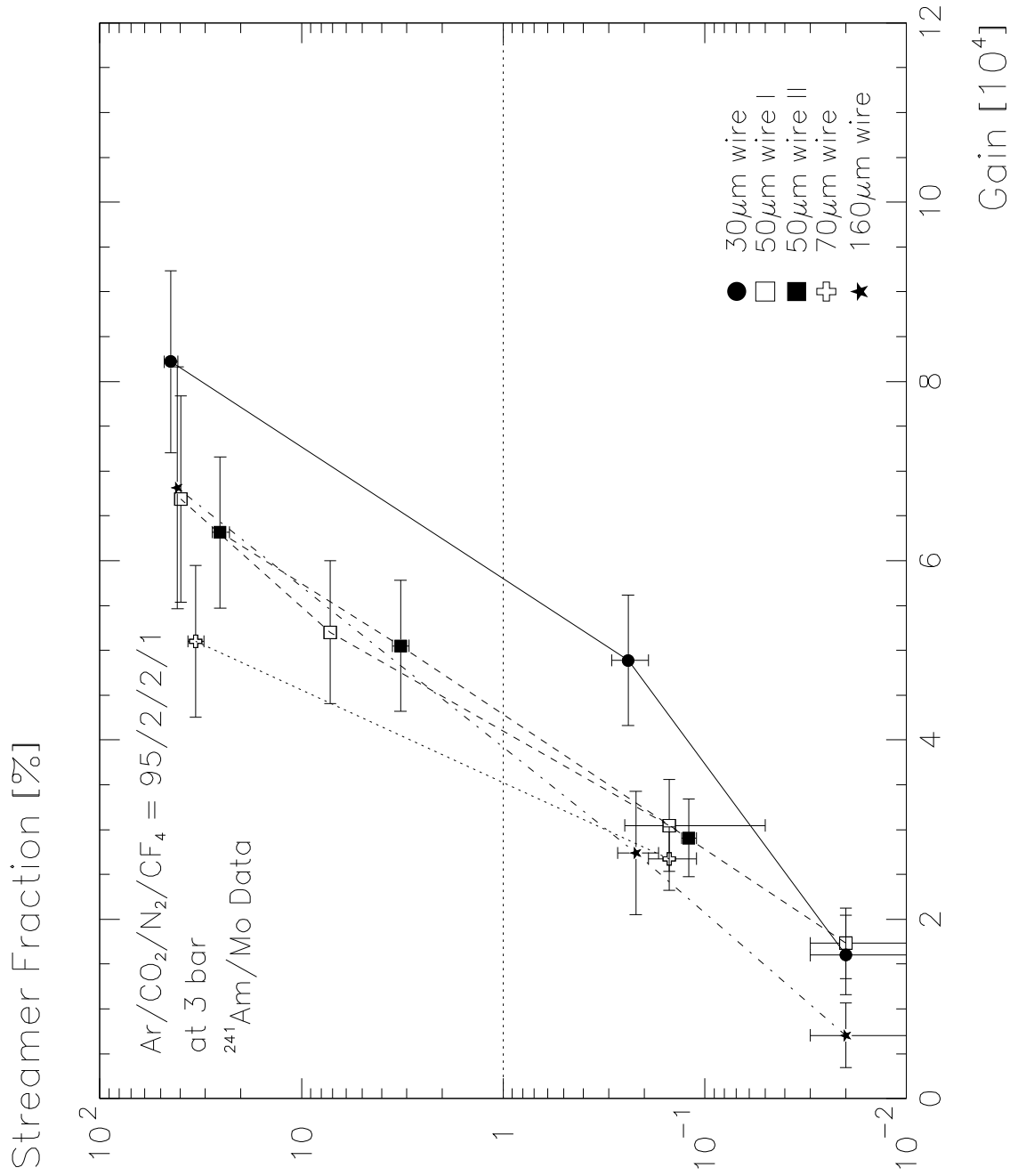
Figure 43: Limited streamer fraction versus gas gain, $Ar:CO_2:N_2:CF_4=95:2:2:1$ at 3 bar, $^{241}Am/Mo$ data.
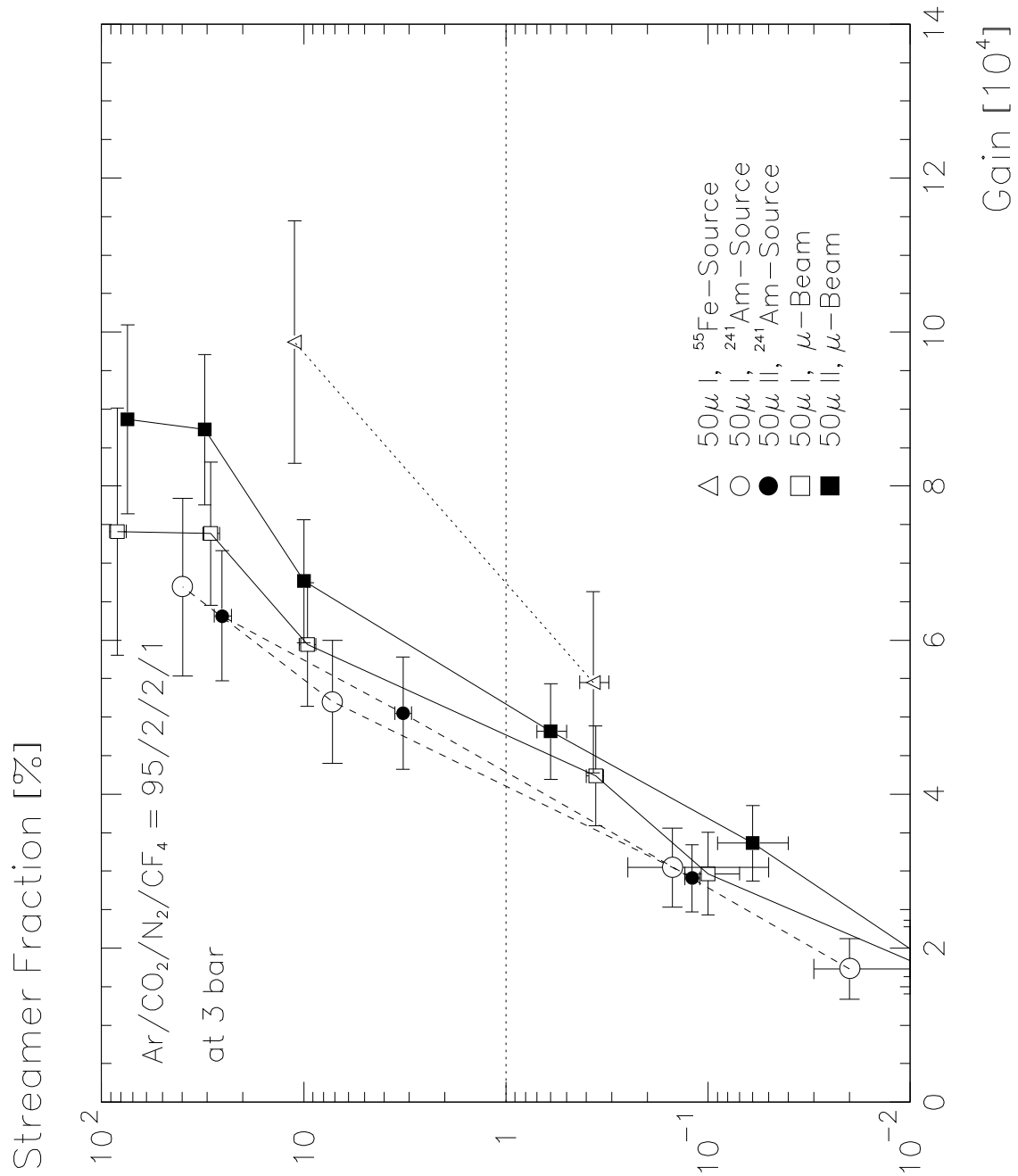
Figure 44: Comparison of the limited streamer fraction versus gas gain, Ar:CO$_2$:N$_2$:CF$_4$=95:2:2:1 at 3 bar, 50 μm wire.
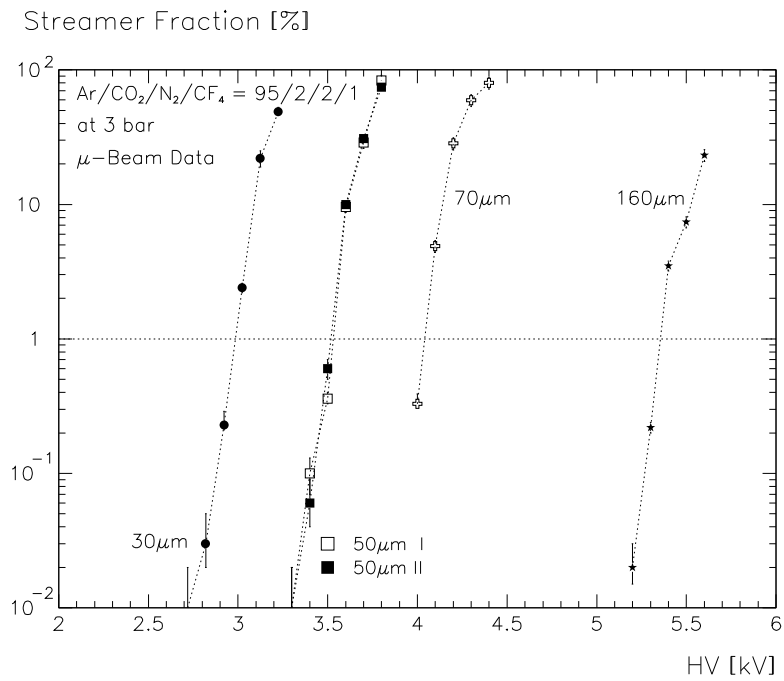
Figure 45: Limited streamer fraction versus HV, Ar:CO$_2$:N$_2$:CF$_4$=95:2:2:1 at 3 bar, μ-beam data.
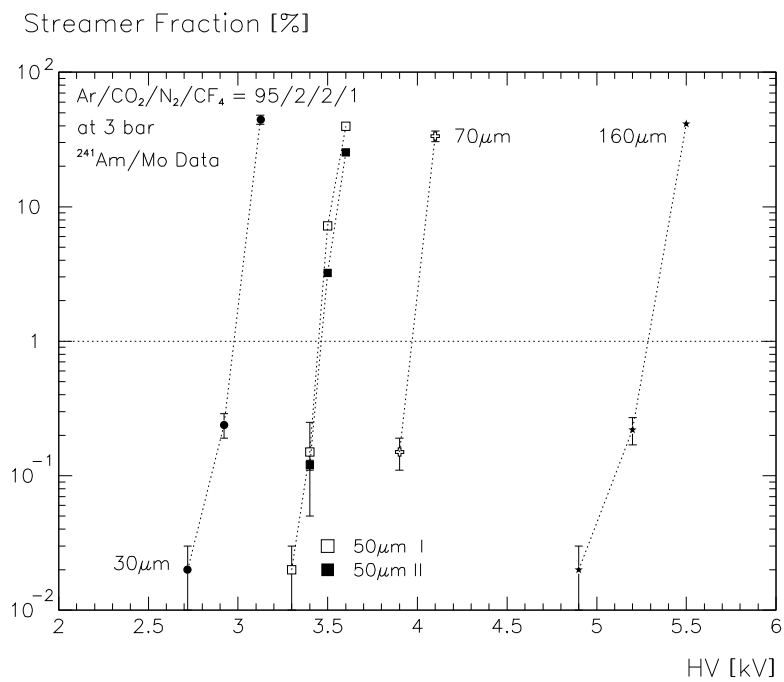
Figure 46: Limited streamer fraction versus HV, Ar:CO$_2$:N$_2$:CF$_4$=95:2:2:1 at 3 bar, [241]Am/Mo data.
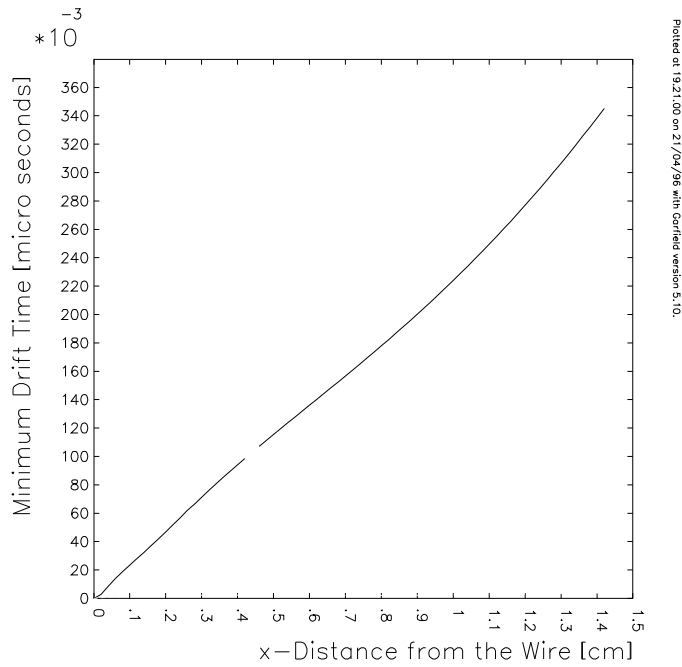
Figure 47: Garfield RT-simulation for $Ar:CO_2:N_2:CF_4=95:2:2:1$ at 3.31 kV (gas gain 2×10^4), 50 μm wire, pressure = 3 bar, temperature = 300 K, magnetic field = 0 T.
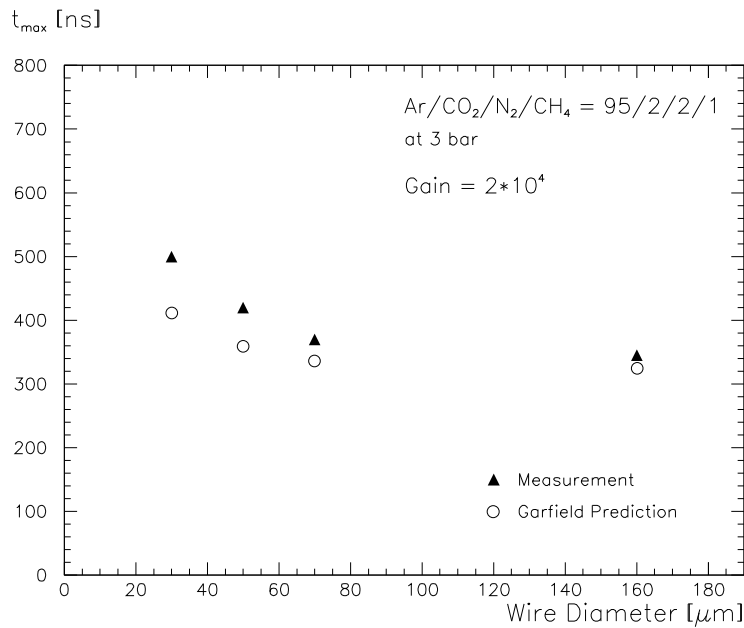

Figure 48: Maximum drift times versus wire diameter for $Ar:CO_2:N_2:CF_4=95:2:2:1$ at 3 bar, gas gain $2 \cdot 10^4$.

8 Summary

The results obtained can help in the choice of gas and wire diameter for both DATCHA (**D**emonstration of **AT**LAS **C**hamber **A**lignment) and the final experiment. We discuss the relative merits of the four gases, with a summary in table 17.

Gas mixture	RT relation	Maximum drift time	After-pulsing	Streamer fraction	Remarks
$Ar:N_2:CH_4$ 91:4:5	linear	short	very low	very low	high streamer charge neutron capture
$Ar:CO_2:CH_4$ 92:5:3	very nonlinear	long	low	medium	unstable working point
$Ar:CO_2:CH_4$ 93:4:3	nonlinear	medium	low	high	low streamer charge
$Ar:CO_2:N_2:CF_4$ 95:2:2:1	slightly nonlinear	very short	high	low	linear at 0.6 T no flammable components

Table 17: Summary of the gases studied, properties are relative to each other.

The $Ar:CO_2:CH_4$ gases were proposed largely for their good ageing properties and it was also claimed they had a low streamer rate. We find the latter not to be the case, but we do see a very much smaller streamer charge than with gases containing nitrogen. Both gases have a non linear rt-relationship, with the $Ar:CO_2:CH_4=92:5:3$ worse than the $Ar:CO_2:CH_4=93:4:3$ mixture. In general rt-relations of non linear gases change more quickly with operational parameters (temperature, pressure, high voltage, etc.) than linear gases, making it harder to maintain good resolution. Especially the $Ar:CO_2:CH_4=92:5:3$ mixture showed large variations in the rt-relationship during data taking. We observed different maximum drift times even for the two 50 μm tubes which differed only by the gas flow rate: the 50 I tube had a longer small diameter gas pipe connecting it to the gas distributor than the 50 II tube. Small contaminations seem to have big effects on the drift properties of these gases. This makes the working point unstable and very hard to control. Furthermore non-linear gases are predicted to have poor resolution at high rates: the increased sensitivity of the electron drift velocity on the electric field leads to bigger changes in the rt-relationship when local variations of ion charges distort the nominal field. For linear gases this effect is much smaller due to saturation of the electron drift velocity.

The $Ar:CO_2:N_2:CF_4=95:2:2:1$ mixture is very promising. It contains no flammable components, enhancing safety. It is very fast, reducing occupancy and reducing the frequency with which one hit obscures another. Both these enhance tracking efficiency. This mixture showed the highest after-pulsing rates of the gases tried, so it would probably be improved by adding more quencher. We recommend studying $Ar:CO_2:N_2:CF_4=90:4:4:2$. The effect of CF_4 on ageing would have to be carefully studied. Also the CF_4 could be replaced by CH_4 which has very similar drift properties.

The $Ar:N_2:CH_4=91:4:5$ gas performed very well. It is linear, has only three components, is non-flammable and has low diffusion. It has a higher streamer charge, which is probably related to the wave length shifting properties of nitrogen. But since the limited streamer fraction is very low this is not a problem. The reaction $^{14}N(n,p)^{14}C$, which produces a 600 keV proton, leads to additional ageing. A pessimistic estimate of the con-

tribution to ageing of this particular reaction is given in appendix A and indicates that the total deposited charge on the wire during operation might be increased by 20%. More detailed calculations are necessary. This mixture should be further studied, especially in a magnetic field and for autocalibration.

One of the goals in finding a gas suitable for DATCHA was to have only 3 components. Then of the gases studied here, the $Ar:N_2:CH_4=91:4:5$ is recommended for DATCHA.

The wire diameter has an impact on many aspects of drift tube performance. Here we just consider one aspect, namely the limited streamer fraction, which for a given gas gain depends on the wire diameter. Limited streamer signals can contain a large charge (up to around 100 times the proportional charge), so that a small streamer fraction can still contribute significantly to ageing. Our results show that at the proposed gas gain of 2×10^4, streamer fractions are low ($\ll 1\%$) for all gases and wire diameters. Even at 4×10^4, they are acceptable ($\lesssim 1\%$) with most gas/wire combinations. This implies that the limited streamer fraction should not be a big factor in choosing the wire diameter: other factors such as resolution, efficiency, ageing and attenuation in long tubes could be more important. However, it should be remembered that the streamer fraction will increase in magnetic fields as tracks from slow charged secondary particles (e.g. δ-electrons) curl up.

Furthermore the effect of wire diameter on streamer fractions is small. The gas gain at which a fixed streamer level is reached seems to have a shallow minimum around 80–90 μm wire diameter. In fig. 49 (a) we plot the gas gain at which the limited streamer fraction reaches the 1% level against the wire diameter for all gases studied. Comparing the dependence of the streamer fraction on the wire diameter between the gases is difficult because of the large fluctuations. To clarify the trend, we average for each wire diameter over the gases, and plot the mean values (filled circles). The gain minimum at around
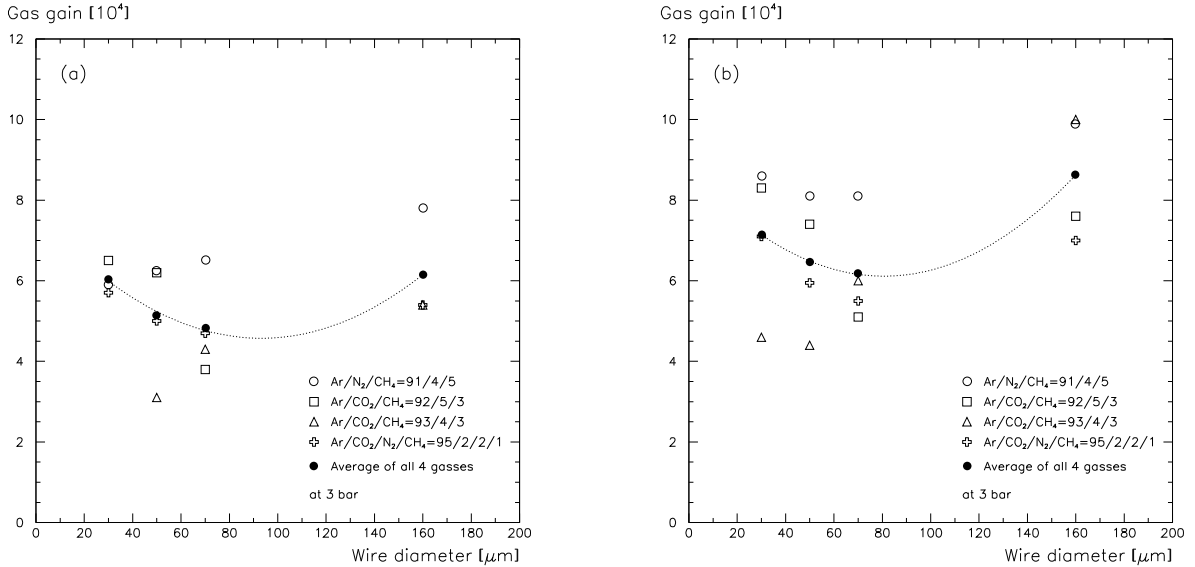

Figure 49: Dependence of the gas gain for fixed limited streamer fraction on the wire diameter. μ-beam data. (a) 1% limited streamer fraction, (b) 5% limited streamer fraction. The filled circles represent the average over all 4 gases. The dotted lines are fitted 2nd order polynomials.

80–90 μm is then clearly visible. Fig. 49 (b) is the corresponding plot at the 5% level of streamers. Again it shows the minimum at around 80–90 μm. The minimum in the gain as a function of wire diameter at a fixed streamer fraction corresponds to a maximum of the streamer fraction as a function of wire diameter at a fixed gain. The fall off of the limited streamer fraction above 90 μm could be a result of the reduction in charge density at the anode: as the wire diameter increases, at a fixed gain, the height above the wire at which the avalanche starts increases. This allows the avalanche to spread more. However, we do not understand why the streamer fraction decreases in the domain 30 μm to 50 μm. The maximum is also apparent in [15], where there is a rise from 50 μm to 70 μm, which flattens so that the 90 μm wire has the same streamer fraction as the 70 μm.

Fig. 49 suggests the wire diameter either be kept small ($\leq 50\mu$m) or large ($\geq 120\mu$m) to minimise streamers. However, as already explained, this will have little influence on the detector performance.

The streamer rates depend on the ionisation mechanism and the primary charge. Higher energy photons create more streamer mode signals than lower energy photons. For muons we observed limited streamer fractions comparable to those of 17 keV photons.

All gases showed less than 1% after-pulsing at a gain of 2×10^4, with the $Ar:CO_2:N_2:CF_4=95:2:2:1$ mixture coming close to this level.

9 Conclusions

With the $Ar:N_2:CH_4=91:4:5$ mixture a good candidate for the final ATLAS gas mixture has been found. It has a stable working point, a linear rt-relationship with maximum drift times around 480 ns and shows only very low limited streamer fractions at a gas gain of $2 \cdot 10^4$. No after-pulsing rates bigger than 1% were observed, even at very high gains. However, we would like to stress that the influence of neutron capture in N_2 on ageing has to be investigated in greater detail. We recommend this gas for use in DATCHA and for further study for possible use in the final ATLAS detector.

The stability of the working point of mixtures containing CO_2 but no nitrogen is questionable, small contaminations seem to have big effects. In addition these gases have a nonlinear rt-relationship which enhances the influence of changes in the operational parameters (temperature, pressure, magnetic field etc.), and give poor resolution at high radiation rates.

At a gas gain of 2×10^4 and zero magnetic field, limited streamer fractions are low ($\ll 1\%$) for all gases and wire diameters. The streamer fraction varies only slowly with wire diameter. Hence the streamer fraction should not be a major factor in the choice of the wire diameter.

10 Acknowledgements

References

[1] The ATLAS Muon Detector Physics Group. Criteria for the Choice of the MDT Operating Point. ATLAS Internal Note MUON-NO-098, CERN, 1995.

[2] M. Deile. Optimierung der Operationsparameter von Hochdruckdriftrohren für ATLAS. Diploma thesis, Ludwig Maximilians University Munich, 1996. Written in German.

[3] V. Gratchev et al. Position and Timing Resolution of Interpolating Cathode Strip Chambers in a Test Beam. ATLAS Internal Note MUON-NO-055, CERN, 1994.

[4] J. Dubbert, N. P. Hessey, L. Pontecorvo, and S. Rosati. RPC setup in the ATLAS Muon Test Area M2. ATLAS Internal Note MUON-NO-085, CERN, 1995.

[5] W. Blum and L. Rolandi. *Particle Detection with Drift Chambers.* Springer Verlag, 1993.

[6] William R. Leo. *Techniques for Nuclear and Particle Physics Experiments.* Springer Verlag, second revised edition, 1994.

[7] P. Rewiersma. *The L3 Wire-Amplifier, Type NH19-6112.* Nikhef, 1986.

[8] P. Rewiersma. *The L3 48 Channel High Speed Discriminator Card, Type NH 19-6523.* NIKHEF, 1986.

[9] N. P. Hessey. The ATLAS Muon Test Beam Data Aquisition System. ATLAS Internal Note MUON-NO-084, CERN, 1995.

[10] M. Deile, J. Dubbert, and N. P. Hessey. Charge Division and Intrinsic Pulse Shaping in Drift Tubes. ATLAS Internal Note MUON-NO-105, CERN, 1996.

[11] H. Fischle, J.Heintze, and B. Schmidt. Experimental determination of ionization cluster size distributions in counting gases. *Nuclear Instruments and Methods A*, A 301(2):202–214, 1991.

[12] R. Veenhof. *Garfield, a drift-chamber simulation program.* CERN, 1996. User's guide Version 5.13.

[13] C. Sartena. Driftröhren. Practicum report, Ludwig Maximilians University, Munich, 1995. Written in German.

[14] T. Zhao and L. He. A Study of Gas Mixtures for ATLAS MDT. ATLAS Internal Note MUON-NO-102, CERN, 1995.

[15] I. R. Boyko et al. Investigation of the ratio between streamer and proportional signals in drift tubes. ATLAS Internal Note MUON-NO-088, CERN, 1995.

[16] A. Ferrari and P.R. Sala. Background rates in the muon system: recent results and the effect of the tungsten plug. ATLAS Internal Note MUON-NO-090, CERN, 1995.

[17] G. A. Chelkov et al. Investigation of the spectral efficiency of pressurized drift tubes for detection of neutrons in the energy range between 5 ev and 200 kev. ATLAS Internal Note MUON-NO-031, CERN, 1993.

[18] S.A. Baranov, I. R. Boyko, G. A. Chelkov, and M. A. Ignatenko. Gamma sensitivity of pressurized drift tubes. ATLAS Internal Note MUON-NO-036, CERN, 1994.

A   Influence of the reaction ^{14}N(n,p)^{14}C on ageing

As mentioned in section 11 another disadvantage (in addition to the higher streamer charge) of nitrogen in gas mixtures is that thermal background neutrons might induce the reaction ^{14}N(n,p)^{14}C which leads to a 600 keV proton.

We estimate the contribution of this particular reaction to the overall deposited charge by assuming a mean cross section over the energy range of thermal neutrons and a constant neutron fluence, thus avoiding cumbersome integrations over the neutron spectrum and the tube volumes.

The reaction rate R is then given by the neutron fluence f (which is defined as the particle track length per unit volume and unit time [16]) times the tube volume V, divided by the mean free path length λ:

$$R \;=\; \frac{f \cdot V}{\lambda} \;=\; f \cdot V \cdot n_N \cdot \sigma \;, \tag{13}$$

where σ denotes the cross section and n_N is the density of nitrogen which is given by

$$n_N \;=\; 2 \cdot \frac{N_A}{V_m} \frac{p_{N_2}}{1 \text{ bar}} \;=\; 2 \cdot \frac{N_A}{V_m} \frac{F_{N_2} \cdot p}{1 \text{ bar}} \tag{14}$$

$$=\; 5.4 \cdot 10^{19} \frac{F_{N_2} \cdot p}{1 \text{ bar}} \text{ cm}^{-3} \;. \tag{15}$$

$N_A = 6.0 \times 10^{23}$ mole^{-1} is Avogadro's constant, $V_m = 22400$ cm^3 is the molar volume and p_{N_2} denotes the partial pressure of nitrogen in bar. The factor 2 takes into account that each nitrogen molecule contains two atoms. We have expressed the partial pressure of nitrogen by the nitrogen fraction F_{N_2} and the gas pressure p in the tube.

We assume (pessimistically) that all protons give rise to a streamer signal. The streamer charge for the similar gas Ar:N$_2$:CH$_4$=90:5:5 has been measured at Seattle to be 400 pC [14, fig. 7].

Multiplying the reaction rate by the charge q of one signal and dividing by the wire length l, we arrive at the deposited charge on the wire per unit length and unit time, $d^2Q/dl\,dt$:

$$\frac{d^2Q}{dl\,dt} \;=\; \frac{R \cdot q}{l} \;=\; f \cdot \pi \cdot b^2 \cdot n_N \cdot \sigma \cdot q \tag{16}$$

$$=\; 1.44 \cdot 10^{-12} \text{ C} \;\cdot f\,[\text{kHz/cm}^2] \cdot F_{N_2}\,[\%] \cdot p\,[\text{bar}] \cdot \sigma\,[\text{barn}] \;, \tag{17}$$

where we have substituted (13) for the reaction rate and made use of the fact that the tube volume is $V = \pi \cdot b^2 \cdot l$ with $b = 1.46$ cm denoting the inner tube radius.

Multiplying $d^2Q/dl\,dt$ by the operation time of the ATLAS MDT in 10 years gives the deposited charge per unit length of wire. We assume a reaction cross section of 1.8 barn over the whole energy range of thermal neutrons, a gas pressure of 3 bar and a nitrogen fraction of 4%. The mean neutron fluence is taken from [16, table 8, case TP 19], which gives a value of 42 kHz/cm^2 for the 1st forward superlayer averaged over the pseudorapidity range $1.44 < \eta < 2.3$. The neutron fluence is scaled by a factor of 1/3

to estimate the fluence of thermal neutrons. The deposited charge per centimetre of wire then evaluates to:

$$Q_{dep,\ N_2} \ = \ 4.4 \cdot 10^{-2} \ \frac{C}{cm} \qquad \text{after } 10^8 \text{ s.} \tag{18}$$

This charge has to be compared with the estimated total deposited charge (muons + background) $Q_{dep,\ total}$ for 10 years at the nominal LHC luminosity. Again, we use the values of [16, table 8, case TP 19] for the calculation. We assume a gas gain of 2×10^4 and a gas pressure of 3 bar. For charged particles (muons, hadrons, $e^{\pm}$) the rate adds to 74 Hz/cm². The mean track length — assuming tracks perpendicular to the tube — is $\delta x = b \cdot \pi/2 = 2.3$ cm. If we assume a primary ionisation of 300 electrons per centimetre, the deposited charge on the wire is 2.2 pC per track. In this case the contribution $Q_{dep,\ charged}$ of charged particles to the total deposited charge per unit length is:

$$Q_{dep,\ charged} \ = \ 4.9 \cdot 10^{-2} \ \frac{C}{cm} \qquad \text{after } 10^8 \text{ s.} \tag{19}$$

For neutral particles we have to distinguish between neutrons and photons, because the tube efficiency is different for these particles. The neutron fluence is 42 kHz/cm² with an average efficiency of 0.2% [17]. The photon fluence is 9.8 kHz/cm² with an average efficiency of 0.5% [18]. We assume that neutral particles liberate 2 times the charge compared to charged particles. This gives a contribution of the neutral particles $Q_{dep,\ neutral}$ of

$$Q_{dep,\ neutral} \ = \ 17.6 \cdot 10^{-2} \ \frac{C}{cm} \qquad \text{after } 10^8 \text{ s.} \tag{20}$$

The total deposited charge is then

$$Q_{dep,\ total} \ = \ Q_{dep,\ charged} + Q_{dep,\ neutral} \tag{21}$$

$$= \ 22.4 \cdot 10^{-2} \ \frac{C}{cm} \qquad \text{after } 10^8 \text{ s.} \tag{22}$$

The contribution of the reaction $^{14}\text{N}(\text{n,p})^{14}\text{C}$ to the overall deposited charge on the wire is therefore:

$$\frac{Q_{dep,\ N_2}}{Q_{dep,\ total}} \ = \ 20 \ \% \ . \tag{23}$$

Please note that this fraction will remain essentially unchanged if the calculation is carried out for a different region of tubes. The absolute values of the deposited charges should be upper estimates since the fluences/rates are highest in the 1st forward superlayer.